FACULTY
OF MATHEMATICS
AND PHYSICS
Charles University

BACHELOR THESIS

Petr Král

Magnetic and transport properties of Yb-based compounds

Department of Condensed Matter Physics

Supervisor of the bachelor thesis: RNDr. Jiří Prchal, Ph.D.

Study programme: Physics

Specialization: General Physics

Prague 2018

I declare that I carried out this bachelor thesis independently, and only with the cited sources, literature and other professional sources.

I understand that my work relates to the rights and obligations under the Act No. 121/2000 Coll., the Copyright Act, as amended, in particular the fact that the Charles University has the right to conclude a license agreement on the use of this work as a school work pursuant to Section 60 paragraph 1 of the Copyright Act.

In Prague 16.5.2018 Petr Král

I would like to express my gratitude to supervisor of my thesis RNDr. Jiří Prchal, Ph.D. for motivation, valuable advice and willingness to devote me his time. I would also like to thank RNDr. Jiří Kaštil, Ph.D. for guidance during measurements, valuable advice on data processing and factual remarks to the text of my thesis. Last but not least, I would like to thank Mgr. Kristina Vlášková for preparation of monocrystalline samples and for her willingness to help me with their characterization.
My thanks belong also to my family and my girlfriend for their support and patience during my study.

Title: Magnetic and transport properties of Yb-based compounds

Author: Petr Král

Department: Department of Condensed Matter Physics

Supervisor of the bachelor thesis: RNDr. Jiří Prchal, Ph.D., Department of Condensed Matter Physics

Abstract: This bachelor thesis is focused on the characterization of Yb_2AlSi_2 compound crystalizing in Mo_2FeB_2-type tetragonal structure. In compounds containing Yb, Ce and U, we can often observe exotic electron features and behaviour, such as non-integer valence, heavy-fermion behaviour or unconventional superconductivity. These properties have the origin in the strong Coulomb interaction in 4f shell and in the hybridization of the f-electron states with conduction electrons. Previous studies were carried out only for polycrystalline samples. The temperature dependence of lattice parameters, electric transport properties, magnetization and heat capacity in external magnetic fields performed on a successfully grown single-crystal are reported in this work. Measurements were done with respect to anisotropy. No trace of any phase transition such as magnetic ordering or superconductivity has been observed. From magnetic measurements the non-integer valence 2.48+ for ytterbium was found. The large, negative $\theta_P^a = -216$ K for magnetic field applied along a ($\theta_P^c = -354$ K for field along c) is a characteristic feature of spin/valence fluctuations. In the study of resistivity, interesting anomaly in current flow along lattice parameter a at temperatures between 150 and 300 K was observed. Another interesting anomaly appears in specific heat temperature dependence below 15 K. Observation of this anomaly together with the enhanced value $\gamma_0 = 153$ mJ mol^{-1}K^{-2} are typical for presence of the heavy fermion ground state of Yb_2AlSi_2.

Keywords: Yb_2AlSi_2, valence state, electrical resistance, magnetization, specific heat

Contents

Introduction

Study of compounds based on rare earth elements attract interest of physical researches. The reason is the effort to enrich our understanding of strongly correlated electron behaviour, which originates from the enhanced interaction between the conduction band and electrons from Yb 4f shell. This behaviour together with extreme conditions is often the cause for new interesting phenomena such as unconventional superconductivity or non-Fermi liquid behaviour [1].

In terms of Yb_2AlSi_2, which is the topic of this thesis, only one study dealing with this compound has been published so far [2]. The authors discussed the influence of substitution on the physical properties of the compound $Yb_2(Mg,Al)Si_2$ (altering Mg for Al). The measurements were carried out on polycrystalline samples, which is given by relatively easy preparation in comparison with the preparation of high-quality single crystalline samples.

In frame of this thesis, measurements of magnetic and transport properties were done on the Yb_2AlSi_2 monocrystalline samples. The biggest advantage is the possibility to measure the physical properties with respect to anisotropy of the crystal lattice. We can combine different directions of current with different directions of external magnetic field with respect to crystal axes.

The thesis is divided into four chapters. The first chapter introduces necessary theoretical terms and physical background of measured features of the sample. In the second chapter, used experimental methods are described. Next chapter summarizes previous results for the studied compound and other compounds based on ytterbium or other rare earth elements. The following chapter contains results of measurements carried out within my work. These results are discussed and compared with previous studies. In the conclusion there is the summary of obtained results.

1. Theoretical background

1.1. The rare earth elements

The rare earth elements (REEs) is a collective name for the group of 17 chemically similar metallic elements between lanthanum ^{57}La and lutetium ^{71}Lu (lanthanide elements) together with scandium and yttrium. These elements are further divided into light REEs (lanthanum, cerium, praseodymium, neodymium, promethium, samarium, europium) and heavy REEs (gadolinium, terbium, dysprosium, holmium, erbium, thulium, ytterbium, lutetium, scandium and yttrium) [3-5].

The chemical similarity originates from the fact that the electron configuration for all of them has the same form [Xe] $6s^2\ 5d^1\ 4f^n$, where n goes from 0 to 14, specifically 13 for ytterbium [6].

Their physical (especially magnetic) properties are very interesting. The differences in magnetic behaviour are caused by the number of electrons in the 4f shell. This number is not changing (with few exceptions) even in the metallic state, because the spatial extent of the 4f shell is smaller than that of the 6s and 5d shells. That's why it doesn't participate in the metallic bonding [7]. If the 4f shell is not fully filled, the localized magnetic moment is formed according to the Hund's rules.

Ytterbium

The studied crystal contains ytterbium ^{70}Yb. This rare earth element was first separated in 1878 and it was called according to the village in Sweden Ytterby, near where it was found. Ytterbium is a soft, malleable and ductile chemical element of the bright silver colour. It is found with other rare earth elements in several rare minerals (monazite, euxenite). Ytterbium crystalizes in the face-centred cubic lattice. It occurs in two oxidation states, most commonly in the 3+ state like the other lanthanides. In this valence state a magnetic moment of $4.54\ \mu_B$ is created by the unfilled 4f shell. Sometimes the Ytterbium also appears in a relatively stable state 2+ which is nonmagnetic due to the fully occupied 4f shell [8].

1.2. Electric transport properties

The electrical resistivity is the fundamental property of metallic materials that express how strongly the material opposes the flow of electric-charge carriers. It is

the process of scattering of conductive electrons on the scattering centres of various origins.

The resistivity ρ of the metallic sample can be expressed by the Matthiessen's rule as

$$\rho = \rho_R + \rho_L + \rho_M, \tag{1.1}$$

where ρ_R is the constant called the residual resistivity and it is caused by scattering electrons on impurities, dislocations, vacancies and other defects, ρ_L is the contribution of thermal phonons and ρ_M is the contribution, which occurs in magnetic materials. Two last mentioned contributions are temperature dependent. The second one is linear for high temperatures ($\rho_L \sim T$) and for low temperatures we have $\rho_L \sim T^5$. The third one is temperature dependent in the magnetically ordered state. In the paramagnetic state the temperature dependence of ρ_M disappears [7,9].

The relationship between the resistance R, which is usually measured by a four wire technique, and the resistivity ρ is given by the following formula, where S is the area of the cross section of the sample and l is the distance of two voltage contacts [10].

$$\rho = \frac{RS}{l} \tag{1.2}$$

1.3. Magnetism

Magnetic properties of matter are well described by quantum theory. The main source of magnetic moment in materials is the magnetic moment of their atoms' unfilled electronic shells. The two components of the magnetic moment are the spin moment of the electrons and their orbital moment. The magnetic moments of nuclei are typically thousands-times smaller [11].

Many electrons in the atom are arranged in the way that their moments cancel out. It is caused by the fact that electrons combine to the pairs with opposite spins. It is the result of Pauli exclusion principle, which says that any pair of fermions can't occupy the same quantum state, i.e. at least one of the quantum numbers should be different. The resulting moment of the fully filled subshell is also zero. Even when the electron configuration is such that there are unpaired electrons or non-filled subshells, the material is not necessary magnetically ordered, because the orientation of magnetic moment of various atoms fluctuate in random directions and their contributions subtract from each other [7,11].

The magnetic field is described by the vector of magnetic intensity $\vec{H}$ and the resulting effect on the matter is given by the magnetic induction $\vec{B}$. In vacuum, they are proportional to each other according to the relation

$$\vec{B} = \mu_0 \vec{H}, \tag{1.3}$$

where $\mu_0 = 4\pi \cdot 10^{-7}\ \mathrm{Hm^{-1}}$ is the permeability of vacuum [11].

When we insert the sample into the external magnetic field the equation (1.3) is modified by the permeability of the inserted material. Depending on the value of the materials permeability we can distinguished different magnetic behaviour.

1.3.1. Diamagnetism

The first option is diamagnetism. It is caused by the effort of electric charge to shield the inside of the sample from the applied magnetic field. This phenomenon is shown in Figure 1.1. (a). The induced moment is opposite to the direction of external field. The negative sign of the magnetic susceptibility is characteristic for diamagnetism.

To describe the diamagnetism of atoms and ions, we can use the Larmor theorem: the movement of electrons around the nucleus in the magnetic field is (in the linear approximation in B) the same as the movement without the field plus the precession of electrons with the angular frequency

$$\omega = \frac{eB}{2m}, \tag{1.4}$$

where $e = 1.60219 \cdot 10^{-19}\ \mathrm{C}$ is the magnitude of the charge of electron, B is the magnetic induction of applied field and $m = 9.10956 \cdot 10^{-31}$ kg is the mass of an electron. The Larmor precession of Z electrons is equivalent to the electric current. The magnetic moment of this current loop with the radius ρ is given as

$$\mu = -\frac{Ze^2B}{4m}\langle\rho^2\rangle, \tag{1.5}$$

where $\langle\rho^2\rangle$ is the mean squared distance between electron and the axis, which is leading through the nucleus and is parallel to the field.

Diamagnetism is a property of all materials and always makes a weak contribution to the material's response to the magnetic field. For materials that show some other kind of magnetism, diamagnetism becomes negligible [7,12].

1.3.2. Paramagnetism

In the second case, the density of field lines in the sample will increase as it is shown in Figure 1.1. (b). The cause of the occurrence of paramagnetism is the presence of uncompensated moment. It is the case of atoms and molecules with odd number of electrons (spin can't be zero), of the free atoms and ions with the partially filled electronic shell (for instance transition elements or REEs).

The magnetic moment of the free atom or ion is given by the relation

$$\mu = -g\mu_B J, \tag{1.6}$$

where $J(L,S)$ is the total angular moment number, $\mu_B = 9.27410 \cdot 10^{-24}$ JT^{-1} is Bohr magneton and $g(J,L,S)$ stands for a so-called Landé g-factor. The effective magnetic moment (the effective number of Bohr magnetons) of the atom can be written as

$$\mu_{eff} = g\mu_B\sqrt{J(J+1)}\,. \tag{1.7}$$

Particularly for Yb in the state Yb^{3+}, when $J = 7/2$ we get the value $\mu_{eff} = 4.54\,\mu_B$. For Yb^{2+} the total angular moment equals $J = 0$ and as a result the $\mu_{eff} = 0$. Other atoms in the studied compound (Al, Si) have also $\mu_{eff} = 0$.

We define magnetization M as the magnetic moment of the unit volume. The magnetic susceptibility of the unit volume can be expressed as a magnetic reaction on the applied magnetic field

$$\chi = \frac{M}{H}. \tag{1.8}$$

For paramagnetic behaviour of the sample, the magnetic susceptibility χ is positive.

On the contrary to the diamagnetism mentioned above, paramagnetic behaviour is temperature dependent. To describe the behaviour in the paramagnetic state we can use the Curie-Weiss law in the form

$$\chi = \frac{C}{T - \theta_P}. \tag{1.9}$$

Here θ_P is the paramagnetic Curie temperature and the Curie constant C has the following meaning [13]

$$C = \frac{\mu_0 N_A \mu_{eff}^2 \mu_B^2}{3k_B}, \tag{1.10}$$

where $N_A = 6.02217 \cdot 10^{23}$ mol^{-1} stands for the Avogadro's constant and $k_B = 1.38062 \cdot 10^{-23}$ JK^{-1} is the Boltzmann constant. From measuring the temperature dependence of susceptibility we can obtain the experimental value of the effective magnetic moment μ_{eff} [7].

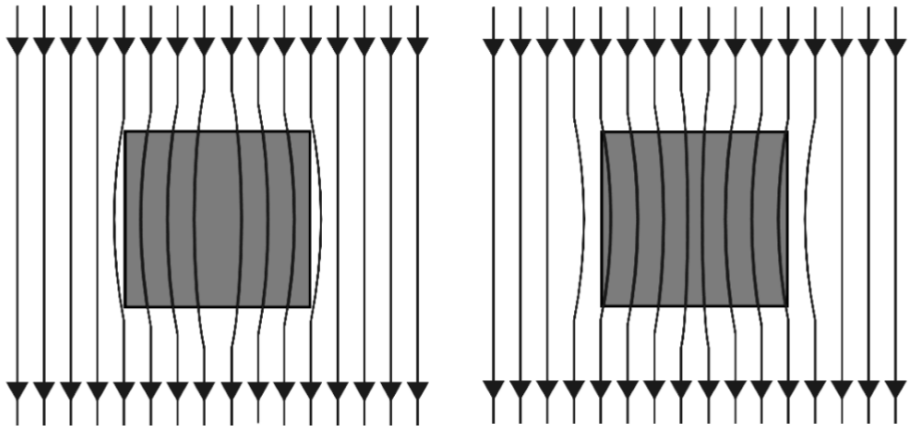

(a) Diamagnetism (b) Paramagnetism

Figure 1.1. Model of diamagnetic and paramagnetic behaviour of the sample in external magnetic field [14]

1.3.3. Magnetic order

According to the mutual orientation of magnetic moments in magnetically ordered state of the material, we can define following types of materials [7,13].

In ferromagnetic materials, resulting magnetic moments are oriented parallel to each other. These materials show the spontaneous magnetic moment, which is nonzero even in the zero applied magnetic field. For every ferromagnetic substance, there exists the nonzero Curie temperature T_C, above which it loses its ferromagnetic properties and the spontaneous magnetization is zero. This temperature separates unordered paramagnetic phase for $T > T_C$ and ordered ferromagnetic phase for $T < T_C$.

In antiferromagnetic materials, the mutual interaction between the magnetic moments is antiparallel, thus the magnetic moments have the tendency to point in the opposite directions. For these materials, the temperature of ordering is called the Néel temperature T_N. For $T < T_N$ the microscopic moments are arranged antiparallel and the resulting bulk magnetic moment is zero. Above T_N the antiferromagnetic substance becomes paramagnetic.

Ferrimagnetic materials are a special case of antiferromagnets with antiparallel orientation of magnetic moments but due to non-equal magnitude of the neighbouring magnetic moments they have got the resulting bulk nonzero magnetic moment also in the zero magnetic field like ferromagnets. Ferrimagnetic order can be caused for example by the fact that there are different magnetic moments from various sublattices – e.g. one formed by transition metal with small moments pointing in one direction than in the other sublattice formed by REEs with the opposite direction of moments.

All of these options are illustratively shown in following Figure 1.2.

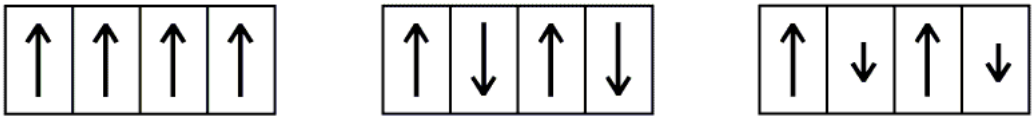

(a) Ferromagnetism (b) Antiferromagnetism (c) Ferrimagnetism

Figure 1.2. Models of magnetically ordered states of the samples [15]

1.4. Specific heat

Specific heat of the material is defined as the heat needed to raise the temperature of the sample of unit mass by 1 K. Heat capacity is the corresponding extensive quantity of the whole sample. According to the type of experiment, we can write the equation in two forms. In the first one, the volume of the sample stays constant during the experiment, the heat capacity is written as C_V. The second option is holding the pressure constant. Then we use notation C_p. For both cases (X stays for V or p) there is the formula

$$C_X = \left(\frac{\delta Q}{dT}\right)_X . \tag{1.11}$$

In experiments, we usually measure C_p, because of the fact that it is easier to hold constant the pressure than the volume of the sample.

It is possible to express the heat capacity in other forms as

$$C_V = \left(\frac{dU}{dT}\right)_V = T\left(\frac{dS}{dT}\right)_V = T\left(\frac{d^2F}{dT^2}\right)_V , \tag{1.12}$$

where U is the internal energy of the system, dS stands for the change of entropy and F is the Helmholtz free energy.

The relation between these two heat capacities is given by the relation

$$C_p - C_V = 9\alpha^2 BVT, \tag{1.13}$$

where α is a coefficient of length expansion, B stands for volume modulus of elasticity, V for volume and T for temperature. The capacity C_p is greater because of the heat used for increasing the volume during the non-isochoric process.

In case of metallic alloys, the specific heat can be written as the sum of individual contributions in the form

$$C_p = C_{ph} + C_{mag} + C_{sch} + C_{el} + C_n, \tag{1.14}$$

where C_{ph} is the contribution of phonons (lattice vibrations), C_{el} stands for the heat capacity of electrons in the sample, C_n for nuclear contribution and C_{mag} and C_{sch} are connected with magnetic interactions [7,9,16,17].

In region of small temperatures, the behaviour of heat capacity can be described using Debye T^3 law in the following form.

$$\frac{C}{T} = \gamma_0 + BT^2 \tag{1.15}$$

In this relation γ_0 is the constant called electronic specific (Sommerfeld) coefficient and the constant B can be written as

$$B = 234 N_A k_B \frac{1}{\theta_D^3}, \tag{1.16}$$

where θ_D is the Debye temperature [7,18].

2. Experimental methods

2.1. Preparation of monocrystal

The used monocrystals of Yb_2AlSi_2 were prepared in collaboration with Mgr. Kristina Vlášková by using the flux growth method. The aluminium self-flux was used and the elements with high purity (Yb purified by using SSE method, Si 6N, Al 6N) were weighed in the atomic ratio Yb:Si:Al = 2:1:20. They were put into an alumina crucible and sealed in silica glass tube with protective argon atmosphere. The mix of elements was heated up to 1100 °C and then cooled down to 900 °C in 14 days, then the remaining Al flux was centrifuged.

2.2. Laue diffraction

To find an orientation of the sample the Laue X-ray diffractometer Photonic Science instrument was used. In this device, there is a special lamp used as a source of the X-ray radiation. An incidental X-ray diffracts on the sample, on the single crystal in this case. The crystal has a fixed position and for each system of planes the parameters d_{hkl} and θ from the following equation are fixed.

$$2d_{hkl}\sin(\theta) = m\lambda \tag{2.1}$$

Parameter d_{hkl} stands for the distance between two neighbouring planes with Miller indexes h, k, l and θ is the angle of incident of X-ray beam.

The diffractometer uses polychromatic radiation. The beam contains appropriate wavelength λ which gives rise to Laue spot in the reciprocal space and according to the equation (2.1) all m create the same spot.
From the resulting pattern we can learn the information about crystal structure of the sample, such as a crystal symmetry along the given direction and its orientation. The pattern reflects a real symmetry of the crystal, it represents the Fourier transformation of the crystal lattice. Points in reciprocal space correspond to the respective systems of planes with the given Miller indexes [7,19].

2.3. Low temperature powder diffraction

The temperature dependence of lattice parameters was measured by LT Diffractometer – D500-HR-4K equipped with a low temperature option provided

by a closed cycle cryocooler (101J Cryocooler ColdEdge) with the measuring range of temperatures down to 4.25 K. This device is using Bragg-Brentano θ-θ geometry with a fixed sample. This geometry allows the use of a divergent X-ray beam with monochromatization or parallelization and therefore avoids losses of intensity due to beam preparation. In the case of the low-temperature XRD a diffraction on a powdered sample is performed. The incident monochromatic beam diffracts on the respective grains which are randomly oriented with equal distribution of the grains orientation. For each angle θ, there exists similar number of grains oriented along the scattering angle. In the case when the Bragg condition (2.1) is fulfilled a diffracted intensity appears and is recorded by the detector [20].

2.4. Electron microscopy

The scanning electron microscope MIRA3 FEG by TESCAN was used to obtain the information about topography and chemical composition of the sample.

The primary electrons impact the sample and can interact in several different ways. The first option is the elastic scattering, when we detect backscattered electrons (BSE). The contrast of images from BSE corresponds to the atomic number of atoms in the sample. The second option is the inelastic scattering, when the energy of primary electron causes the release of an electron from the atom of the studied sample. These electrons are called secondary electrons (SE) and they have got low energy in comparison with BSE. They give the information about the topography of surface. The incident electrons can also excite electrons from the inner shells and then we detect the characteristic radiation coming from the recombination of electrons between the electronic energy levels back to the ground state. The set of frequencies coming from these transitions between the electronic energy levels is typical for each element. This method is called energy dispersive X-ray analysis (EDX). From the corresponding spectrum it is possible to obtain the information about the chemical composition of the studied sample.

The disadvantage of this method is the fact that due to low penetration depth, only the surface composition can be estimated and we cannot obtain information about the whole sample [9,21].

2.5. Resistivity measurement

To measure the electric transport properties the Physical Property Measurement System (PPMS) by Quantum Design was used. This device provides the possibility to measure various physical quantities including the electric resistance in the temperature range from the room temperature down to 2 K. It is also possible to apply the external magnetic field up to 14 T [22].

For the measurement it is necessary to contact the sample in the four-point configuration to eliminate the influence of wires. It means that we contact it with two voltage and two current wires as shown in Figure 2.1. Due to quite small proportions of the sample, an optical microscope is necessary. The sample was fixed to the special puck by a GE varnish (special low-temperature glue) and electrically insulating pad. Then we use micro-welding to make electrical contacts between the sample and the gold wires. In the case of sample Yb_2AlSi_2 C, also the silver paste was used.

For measurements down to 0.38 K we used the special additional device to PPMS which works with He3 and high vacuum.

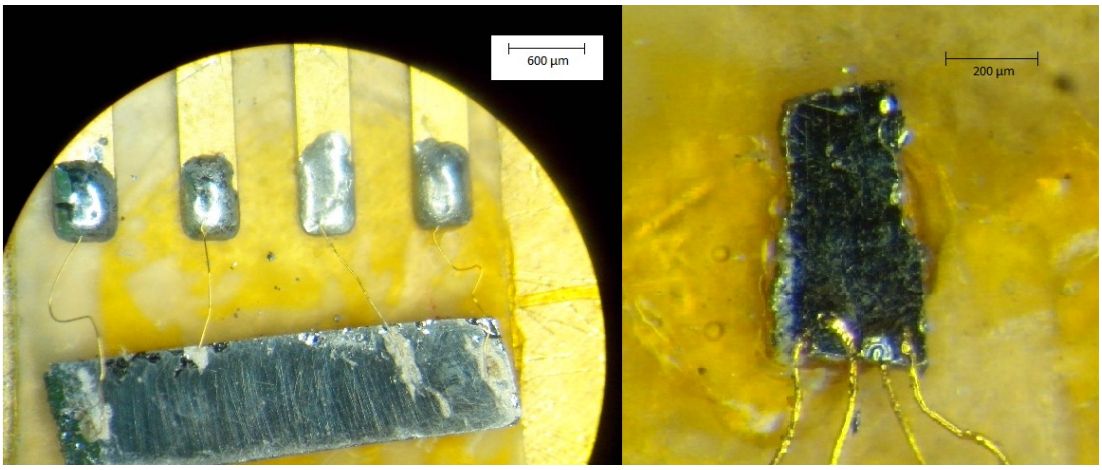

Figure 2.1. The samples prepared for electric resistance measurement (Yb_2AlSi_2 C left – for current flow along c and Yb_2AlSi_2 A right – for current flow along a)

2.6. Magnetization measurement

The magnetization measurement (measuring of the magnetization with the external magnetic field applied along the lattice parameter c), was also carried out in PPMS using Vibrating Sample Magnetometer (VSM). It is also possible to measure the magnetization in temperatures down to 2 K and to apply the external magnetic fields

up to 14 T. To prepare the sample for measurement, we use the special glass bar and mounted a sample on it by the GE varnish. PPMS uses the Faraday induction law to get the response of the sample on the movement in external magnetic field. The sample is being moved in the detection coils set and as a consequence, the induction of signal (voltage) is measured. This is analysed by the software and as the output we get the value of magnetic moment [23].

In terms of measurement with magnetic field applied along a, Magnetic Property Measurement System (MPMS) by Quantum Design was used. This device is intended for measuring the smallest magnetic moments. This method uses the superconducting detection coils and SQUID (Superconducting Quantum Interference Device) to precisely determine magnetic moment of the sample [24].

For our measurement of magnetization the sample was oriented either along the a direction or along the c direction with respect to the magnetic field.

2.7. Heat capacity measurement

The heat capacity measurement was carried out on PPMS device by Quantum Design (the same device was used for resistance measurements and one part of magnetization measurement).
The Heat Capacity option measures the heat capacity at constant pressure. The sample is attached to an insulated platform in the special puck by thin layer of Apiezon grease. The puck contains the thermometer and the heater on its bottom side. The puck with the sample is then placed into the chamber and high vacuum is applied. The measurements were performed by the relaxation heat-pulse method. It means that the temperature is stabilized at the given base temperature. Then the defined heat-pulse increases the temperature of the platform and the sample (2 % of the base temperature in our case) and the relaxation of the temperature with time is measured [25]. Figure 2.2. (a) shows the puck and Figure 2.2. (b) shows a measuring cycle for one pulse.

Before the measurement itself, the addenda was measured. It means that we measured the temperature dependence of heat capacity for Apiezon in the exact amount used to attach the sample later on. This contribution together with contribution of the whole puck have to be subtracted from the measured (total) heat

capacity. We describe these steps for clarity, nevertheless all these calculations are processed by the software.

(a)

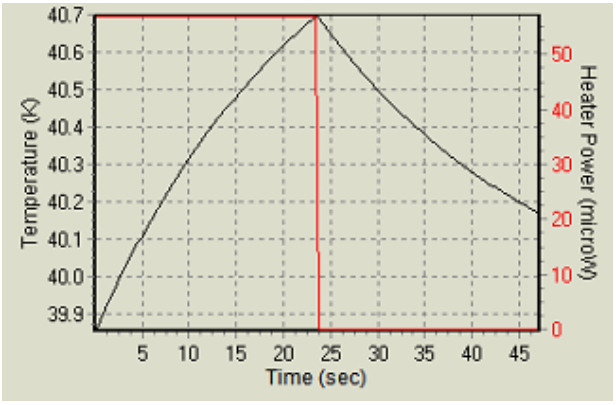

(b)

Figure 2.2. The heat capacity puck used for measurement on PPMS in (a) and the typical measuring cycle – red line shows the heat pulse and the black one the temperature evolution of the sample (b)

3. Previous results and motivation

Studying Yb-based compounds is important to enrich our understanding of the strongly correlated electron behaviour, which is caused by an enhanced interaction between the conduction electrons and the local Yb 4f moment.

The topic of strongly correlated electron systems and quantum criticality has received great attention, because of the appearance of many interesting new phenomena connected with the quantum critical point (QCP). As an example we can mention unconventional superconductivity or non-Fermi liquid behaviour.

In order to bring compounds to the QCP usually external magnetic field and/or the hydrostatic or chemical pressure is needed to apply.

Intermetallic compounds containing Ce, Yb and Eu are known to exhibit non-integer valence. For instance in YbPd compound, 2.66+ valence of ytterbium was observed [26].

Previous measurements of structural and magnetic properties were carried out on polycrystalline samples. It could be interesting to prepare and study monocrystalline samples, because of the possibility to measure the physical properties in different directions and study the anisotropy of these properties including application of hydrostatic or uniaxial pressure.

Experiments on polycrystals of the $Yb_2Al_{1-x}Mg_xSi_2$ compounds were executed for $x = 0, 0.5$ and 1 to study the effect of chemical pressure on the compound, because of the diametrically different features of magnetic ground states of these compounds [2].

Both Yb_2AlSi_2 and Yb_2MgSi_2 crystallize in the tetragonal Mo_2FeB_2-type structure. The lattice constant a is growing from 6.7331(4) Å for $x = 0$ to 7.0530(6) Å for $x = 1$. Also the volume of the unit cell is increasing with this substitution, from 194.52(5) $Å^3$ to 205.52(8) $Å^3$. The parameter c is decreasing from 4.2403(4) Å for the aluminium compound to 4.1282(5) Å for the sample containing magnesium.

In terms of the magnetic properties, the susceptibility in Al compound increases monotonically with decreasing temperature and there is no signature of a magnetic transition. Between 200 and 300 K susceptibility follows nearly a Curie-Weiss behaviour with $\mu_{eff} = 4.2\ \mu_B$ and $\theta_P = -203$ K. The large, negative θ_P is a

characteristic feature of spin/valence fluctuations. The strong 4f conduction band hybridization gives rise to Pauli paramagnetic ground state [2].

The electrical resistivity of paramagnetic Yb_2AlSi_2 shows a slight negative temperature coefficient between 200 and 300 K and drops gradually bellow 100 K.

As for the heat capacity of Yb_2AlSi_2, the monotonic decrease with temperature down to 1.8 K was observed. In C/T plot an interesting upturn below 12 K can be observed as a precursor of a magnetic transition but a magnetic origin of the upturn can be ruled out, because C doesn't show any upturn.

In terms of other compounds containing ytterbium, the studies concerning $YbAu_2Si_2$ or $YbCu_2Si_2$ for example were carried out [1,27].

Due to the $4f^{13}$ configuration, Yb is considered as a hole analogue of Ce. In cerium compounds, superconductivity is often observed. On the other hand, observations of superconductivity in Yb compounds are rare. It is sometimes ascribed to dominant ferromagnetic exchange in some Yb-based systems. For example ferromagnetic ordering in the above-mentioned $YbCu_2Si_2$ under external pressure above 8 GPa has been observed [27].

Measurements carried out on polycrystalline samples of $YbAu_2Si_2$ have shown that this compound is non-magnetic metal with Yb in 2+ state. A tiny magnetic contribution is probably caused by the small amount (2 %) of Yb 3+ present in the sample. It was not decided if trivalent Yb atoms are part of the pure sample or present as an impurity.

4. Results and discussion

4.1. Characterization of the sample

4.1.1. Laue diffraction

The orientation of monocrystalline samples was checked by Laue diffraction. For all measurements carried out on monocrystals, two samples were chosen. These samples were named Yb_2AlSi_2 A and Yb_2AlSi_2 C, according to their future use.[1]

On Figure 4.1., there is shown a Laue diffractogram for the second named sample for X-rays impacting Bragg plane 1 0 0.

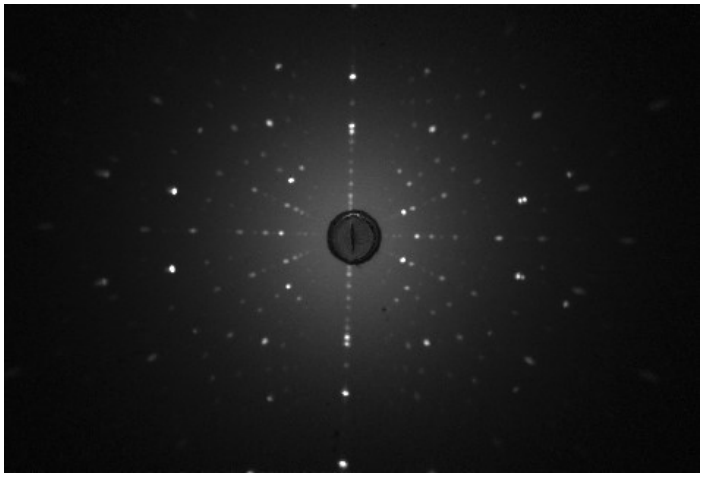

Figure 4.1. Laue diffractogram for Yb_2AlSi_2 C for Bragg plane 1 0 0

4.1.2. Low temperature diffraction

To study the temperature dependence of the lattice parameters, we use the low temperature diffraction. The diffraction pattern was fitted using the software FullProf developed in ILL Grenoble [28].

The diffraction pattern for 300 K is shown in Figure 4.2. From the analysis of the measured data we have refined the lattice parameters at 300 K $a = 6.7681(4)$ Å and $c = 4.2356(3)$ Å and we verified the fact that studied compound crystalizes in the expected P4/mbm tetragonal structure.

---

[1]Their orientation is demonstrated later in the subchapter 4.1.3 on Figure 4.4.

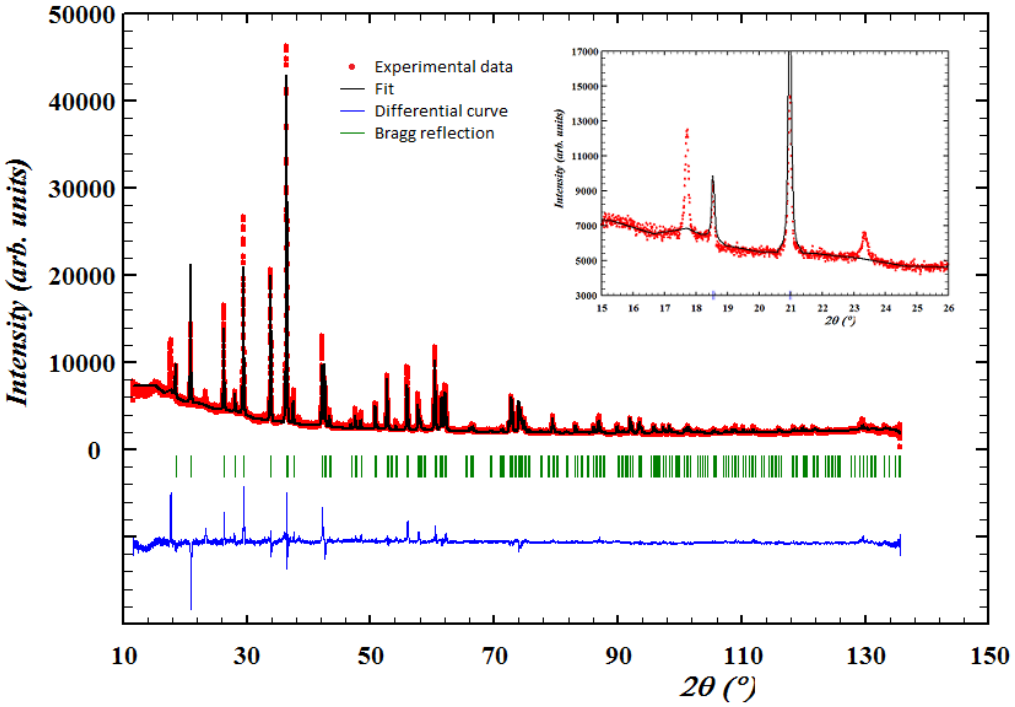

Figure 4.2. Refinement of the X-ray pattern of Yb_2AlSi_2 at 300 K analysed by FullProf.

In the inset in Figure 4.2., one can see two peaks that don't belong to any Bragg reflection from the expected structure. These peaks can indicate presence of some oxide impurity phases.

Figure 4.3. summarizes obtained results for the temperature development of the lattice parameters.

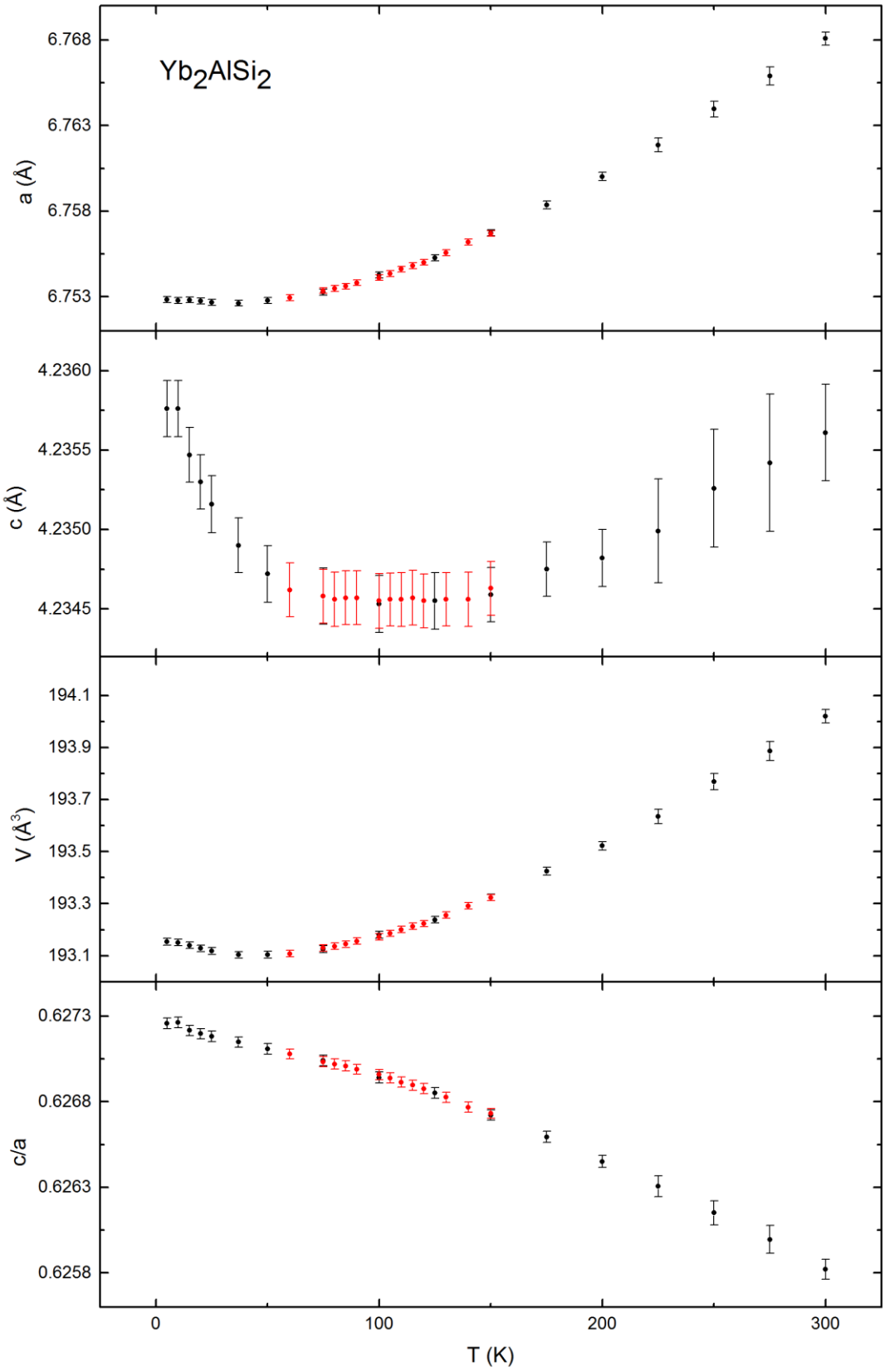

Figure 4.3. Temperature dependence of lattice parameters obtained by low-temperature diffraction. The data in red correspond to the repeated measurement (see text).

Temperature range from 5 K to 300 K and between 60 K and 150 K the measurement was repeated with the smaller step.

As we can see, the dominant parameter for temperature development of the crystal is lattice parameter a. Under the temperature about 50 K it is almost constant and for higher temperatures we can observe an increase of its value, approximately 0.09 % per 100 K.

On the other hand parameter c changes very weakly with increasing temperature. It is possible to see the local minimum at about 100 K, but the changes in the value of c are cca ten times smaller than in the case of a. In the temperatures where the parameter a is nearly constant, c has the tendency to increase with decreasing temperature.

In terms of volume of the unit cell, we can see that for temperatures corresponding to the area where parameter a is growing the influence of changes in c doesn't play a role and the volume behave in the same way as a. For lower temperatures, approximately under 50 K, an effect of growing parameter c starts to be visible. As the consequence we can observe the slight increase of the volume during decreasing temperature and that's why it gives rise to the minimum at temperature about 35 K.

The dependence of ratio c/a is shown in the last graph in Figure 4.3. Here we can see the decreasing tendency, which is caused by the main influence of changes in a. In comparison with development of a, changes of c are negligible. We divide nearly constant value by the increasing value of a. The small trace of the effect of c we can observe bellow 10 K, where the tendency seems to be growing.

4.1.3. EDX analysis

Stoichiometry and homogeneity of prepared samples were checked using EDX analysis. Stoichiometry was checked in several points (6) on both samples. As the result we determined that the stoichiometry is not exactly Yb: Al: Si = 2: 1: 2, but Yb: Al: Si = 2: 1.3: 1.7 for the sample Yb_2AlSi_2 A and 2.1: 1.2: 1.7 for Yb_2AlSi_2 C (given as the mean value of all measured points). However the stoichiometry does not corresponds well with the desired composition of 2:1:2 phase, we can say that the stoichiometry is nearly the same for both samples in all checked points. With respect to the error of this method which is about 2%, we cannot consider the sample to be

$Yb_2Al_1Si_2$. However the mutual substitution between Al and Si can have significant effect on the physical properties we will refer the samples as Yb_2AlSi_2 for simplicity of the text. As for the homogeneity, we can see that the samples are well homogenous. This fact is shown by spectra for Yb_2AlSi_2 C in Figure 4.5. In this figure we can see that the intensity curve is nearly the same for each examined point. The same result was received for the second sample. For both samples also mapping was done and the results are summarized in Figures 4.6. and 4.7. No trace of foreign phase had been detected apart from the remainder of Al flux with the possible phase $YbAl_3$ in the sample Yb_2AlSi_2 A, which can be seen in Figure 4.6. as the area with the higher amount of Al in the right part of the sample. This impurity doesn't pose a problem, because it is located at the edge of the sample and this area isn't used in any other measurement.

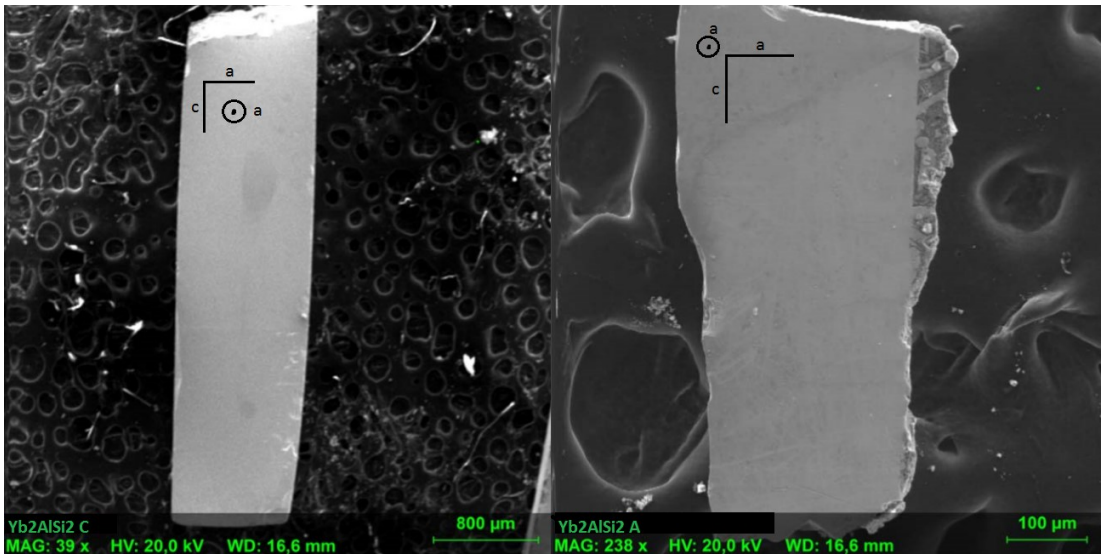

Figure 4.4. Orientation and proportions of used monocrystalline samples

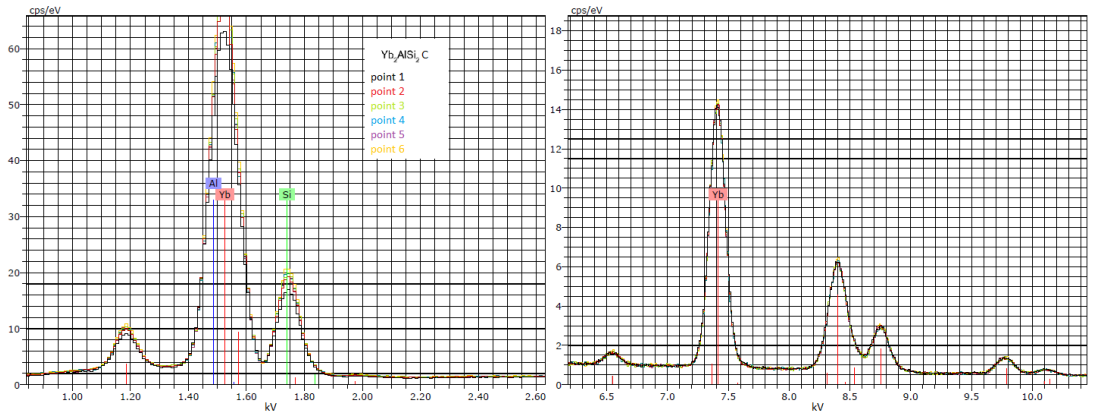

Figure 4.5. EDX spectra for Yb_2AlSi_2 C

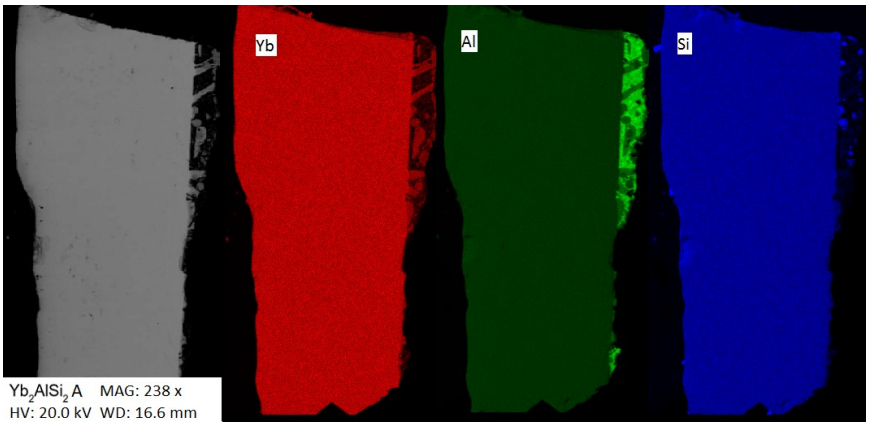

Figure 4.6. Mapping for Yb_2AlSi_2 A

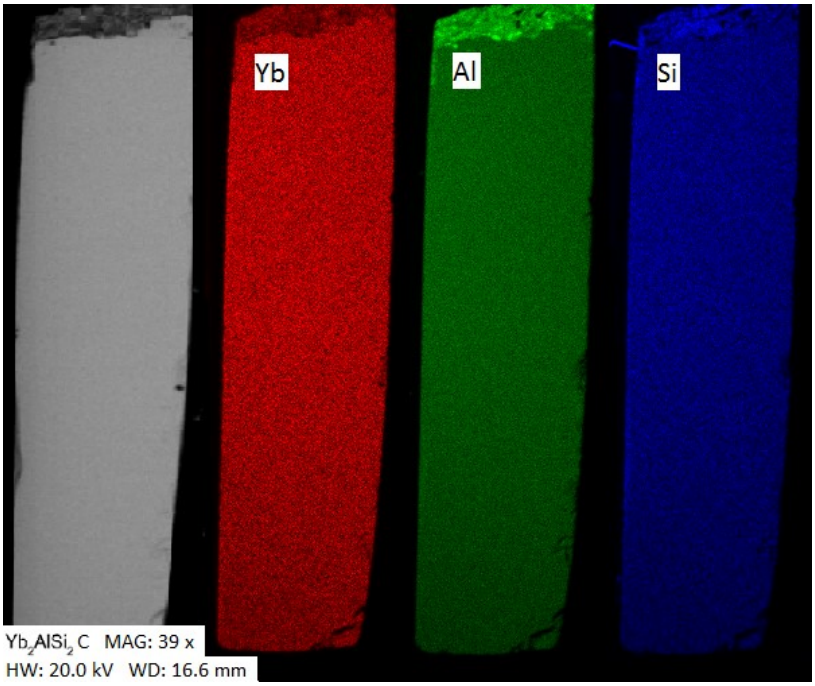

Figure 4.7. Mapping for Yb_2AlSi_2 C

4.2. Resistivity measurement

Measurement of the resistance was done for both samples "Yb_2AlSi_2 A" (current flow along a) and "Yb_2AlSi_2 C" (current flow along c). External magnetic field was applied in transversal configuration along a in both cases. Because of not ideal shape parameters of the first mentioned sample, only the ratio R/R_{300} (where R_{300} stands for the resistance in temperature 300 K) is given in Figures 4.8. and 4.9. for both directions of current. The resistivity obtained from the equation (1.2) is shown only for the bigger sample "Yb_2AlSi_2 C" with properly estimated shape parameters. We

measured the temperature dependence of resistance for various values of external magnetic field.

In Figures 4.8. and 4.9., we can observe the anisotropy in the temperature dependence of resistance behaviour.

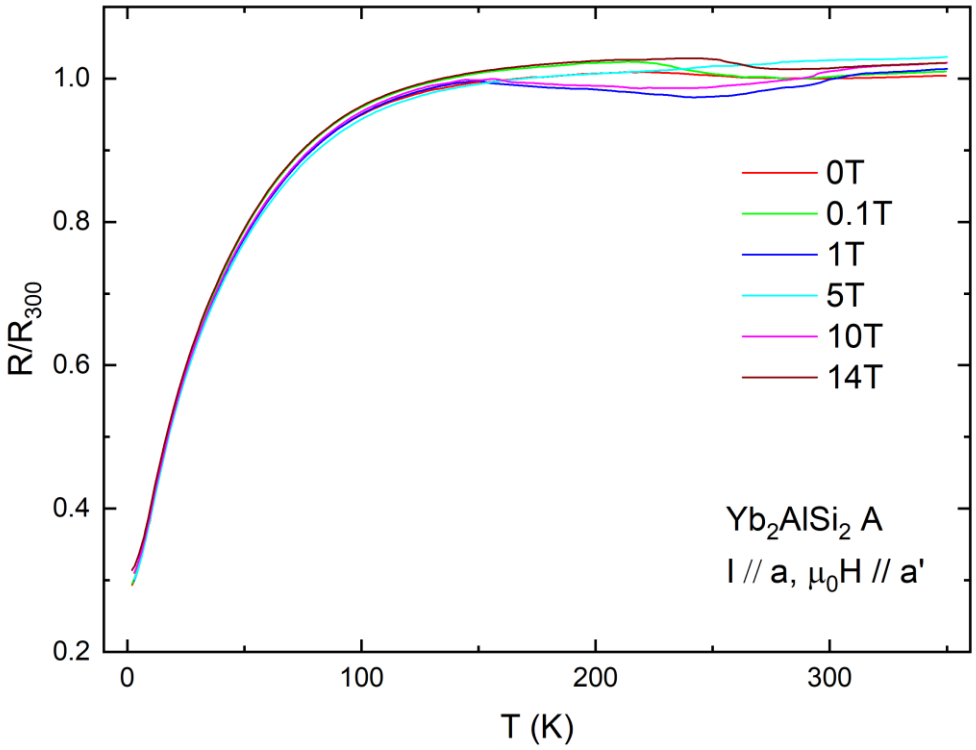

Figure 4.8. Temperature dependence of R/R_{300} ratio for current direction along lattice parameter a and the transversally applied external magnetic field along a'

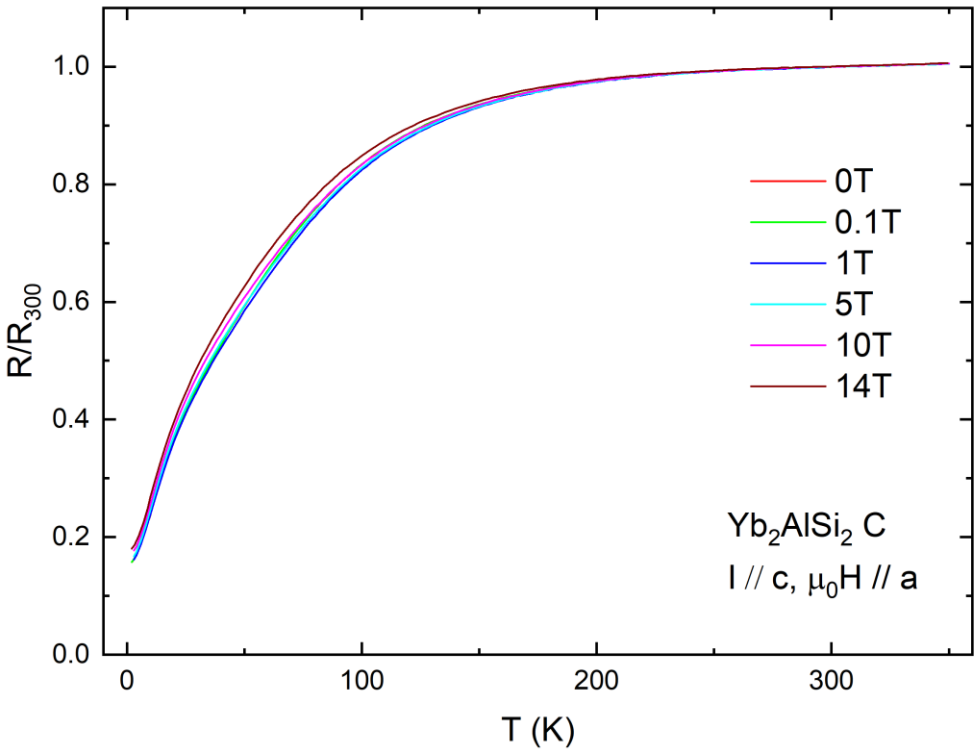

Figure 4.9. Temperature dependence of R/R_{300} ratio for current direction along lattice parameter c and the transversally applied external magnetic field along a

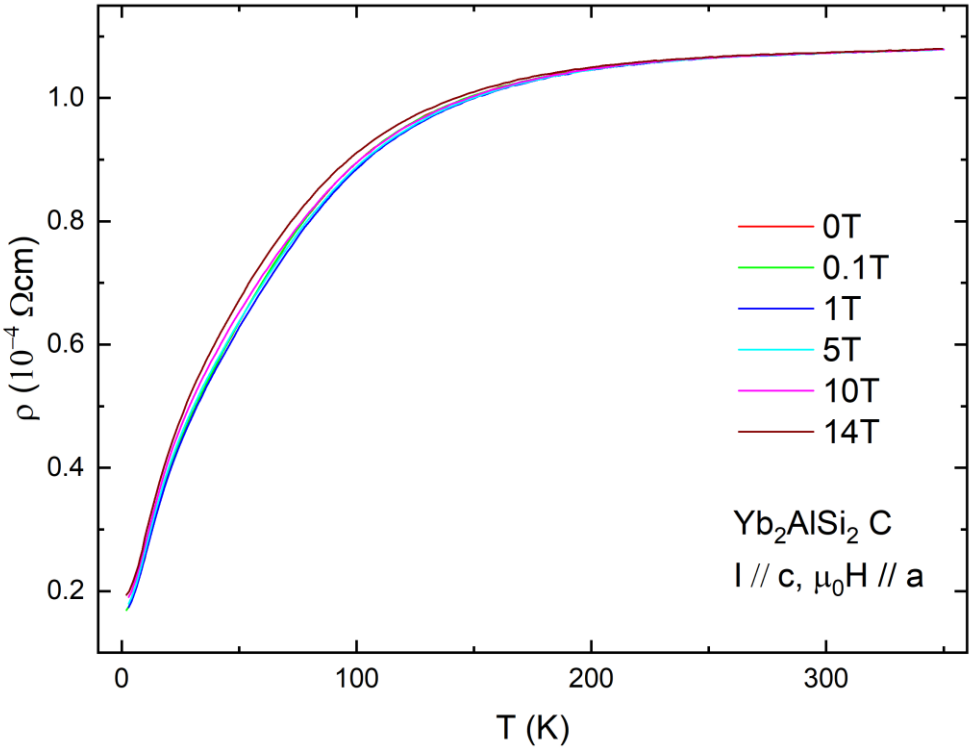

Figure 4.10. Temperature dependence of resistivity for current direction along lattice parameter c and the transversally applied external magnetic field along a

For the current along the direction c, we can see the monotonous increase of the ratio R/R_{300}. Above 300 K, the ratio dependence continues monotonically over the value

1. Below 200 K there are differences in the shape of curves for various magnetic fields. Above 150 K, all curves besides curve for 14 T, which joins for temperatures over 200 K, merge into one curve. In terms of this external field dependence of the curve shapes, the curves for 0 T and 0.1 T are nearly the same. The dependence for zero field was measured both for increasing and decreasing temperature, without any observed difference. For higher fields, there appears deflections from the zero field curve. The curve for 1 T lies lower, the curve for 5 T lies between two previous and for 10 T and 14 T, the position of curve is increasing over the zero field curve with growing field.

On the other hand for current along a, we observe monotonous increase, which has got the higher slope than in the case of current along c, but only in the temperature region below 150 K. Differences between curves for various magnetic field occur for the whole temperature range, where the measurement was carried out. Above 150 K the differences are larger and more peculiar. In this region we can observe even the decrease of the curves and for some fields, there appears a local minimum. The biggest decrease can be observed for 1 T field, the smallest for 5 T field. Also the dependence on the temperature evolution is present. The zero field curve was also in this case measured for increasing and decreasing temperature and we can observe the difference here. For decreasing temperature the curve lies lower.

In Figures 4.11. and 4.12., there is shown the temperature dependence of electric resistivity (in the form R/R_{300}) in external magnetic field for both increasing and decreasing temperature in the range between 0.38 and 20 K in He3 option on ETO PPMS. From dependences for the current flowing along a and c (the same parameters of measurement as in the previous, transversal magnetic field), we can say that the shape of curves corresponds also in these low temperatures with what we could see above. For current flow along a, we observe the higher slope of curve. Another sign of anisotropy is the fact that R_0/R_{300} as the value of extrapolation the ratio to the zero temperature is different for each direction of current, although it is necessary to remember that different samples were used for measurement in different orientation. For current along a, the value is higher (curves lead to the value near 0.3). On the other hand, for current along c, however the slope is lower, the resulting value is under 0.2 for all curves.

For both directions of current, we didn't observe any sign of any transition. Curves are smooth for the whole temperature range.

If we compare the region between 2 and 20 K, which is common for ETO and ETO He3 measurement, we can see that there are no differences in the shape of dependences. Only difference is the fact that curves from ETO lie little bit lower. However this fact does not pose a problem, much more important is the shape of the curves. The small shift of absolute values is not uncommon for measurement performed in different conditions.

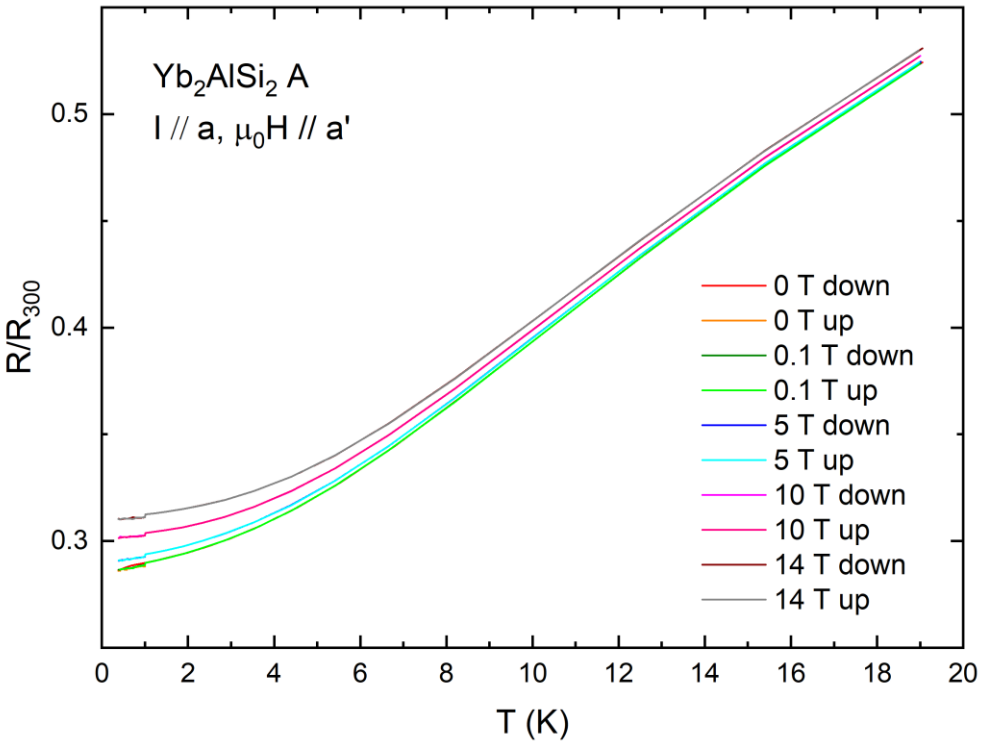

Figure 4.11. Temperature dependence of R/R_{300} ratio for current direction along lattice parameter a and the transversally applied external magnetic field along a' for lower temperatures obtained by PPMS ETO He3 option

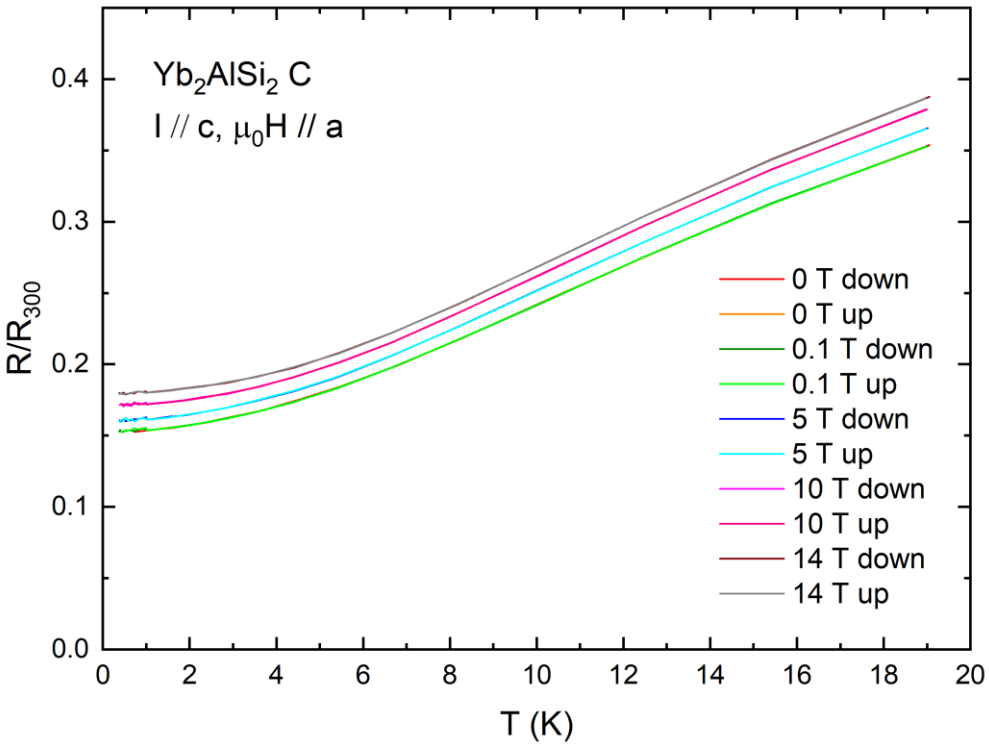

Figure 4.12. Temperature dependence of R/R_{300} ratio for current direction along lattice parameter c and the transversally applied external magnetic field along a for lower temperatures obtained by PPMS ETO He3 option

4.3. Magnetic study

4.3.1. Magnetization

Magnetization of the sample was measured for various values of external magnetic field in wide temperature region and also the dependence on applied magnetic field for various constant temperatures (the magnetization curves) was recorded. Both measurements were carried out on the sample "Yb_2AlSi_2 C" with external field applied first along c-direction on PPMS and then along a-direction on a MPMS magnetometer. Which is the reason why the range of magnetic field goes up to 14 T for $\mu_0 H \,//\, c$ and only up to 7 T for $\mu_0 H \,//\, a$. The results of magnetization measurements are shown in following figures.

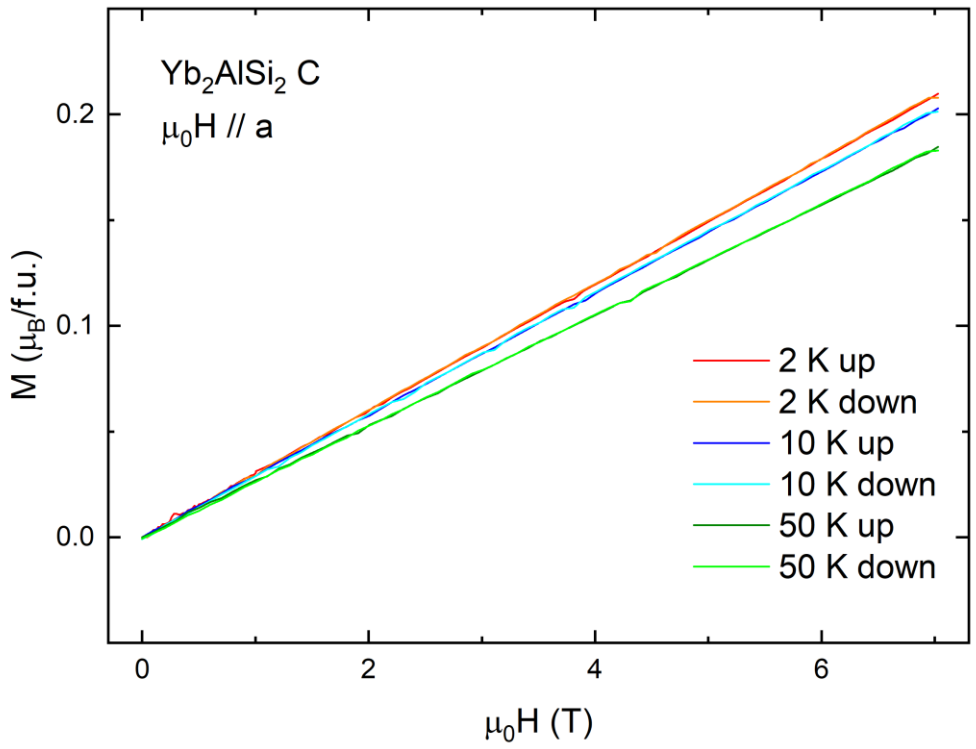

Figure 4.13. Magnetization curves for various temperatures and both increasing and decreasing external magnetic field applied along lattice parameter a

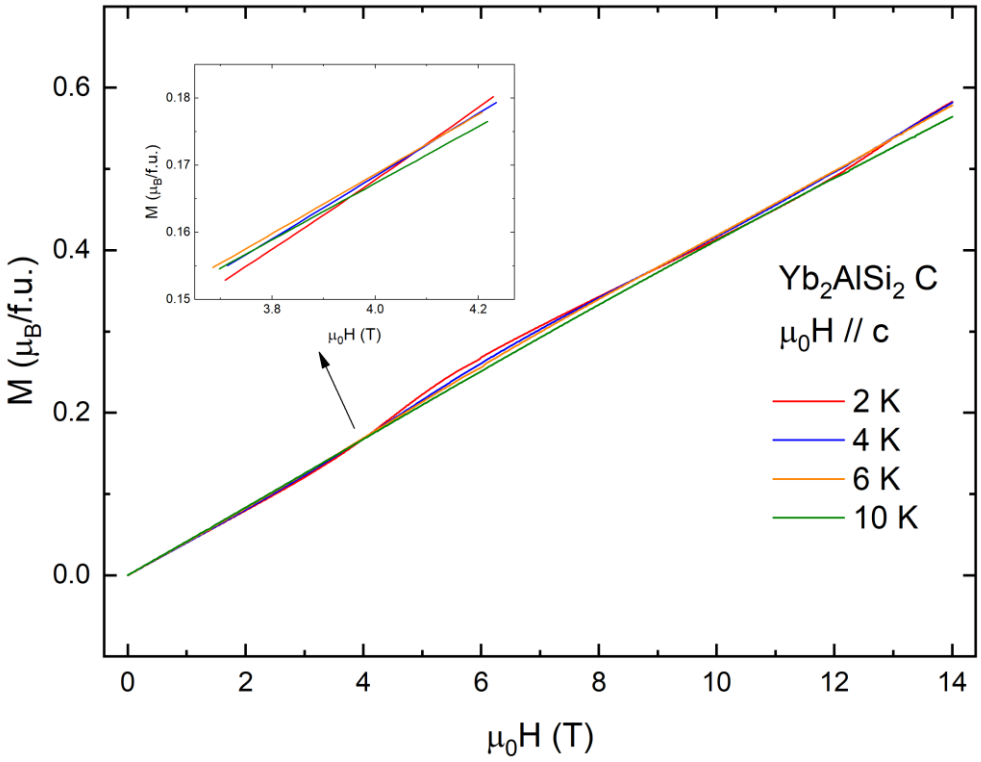

Figure 4.14. Magnetization curves for various temperatures and both increasing and decreasing external magnetic field applied along lattice parameter c with detail of the area around 4 K in the inset

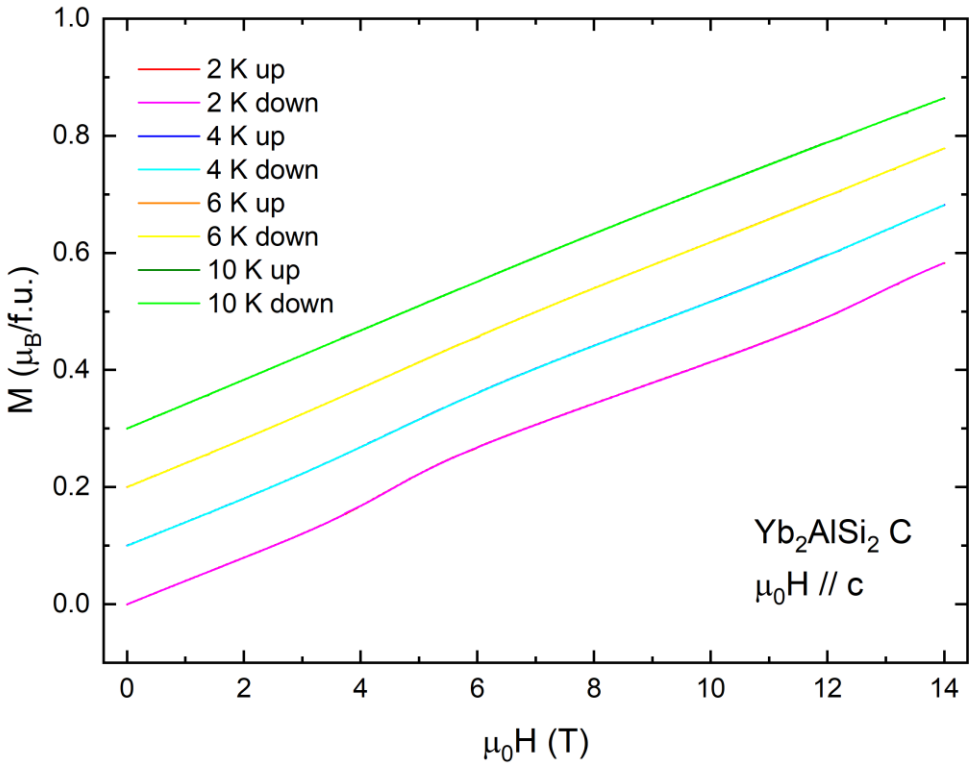

Figure 4.15. Magnetization curves for various temperatures and external magnetic field applied along lattice parameter c shifted 0.01 $\mu_B/f.u.$ vertically

In Figure 4.13., there is shown the dependence of magnetization on external magnetic field applied along a-direction. Measurement was carried out in various temperatures. We can observe the linear tendency for all of these temperatures in the whole region of magnetic intensity, in which the measurement run through.

In Figure 4.14., there is shown the dependence of magnetization on external magnetic field along c-direction. The inset shows the interesting area around 4 T.

In Figure 4.15., previous curves are shifted for higher lucidity. We can observe interesting non-linear dependence with two "waves" in measured range (one of them for 4 T was discussed above, the second lies around 11 T). For higher temperatures these deflections from linear tendency disappeared. The linear behaviour is almost recovered for 10 K curve.

4.3.2. Magnetic susceptibility

Magnetic susceptibility temperature dependence was obtained from measurements of the temperature dependence of magnetization in various external magnetic fields according the relation (1.8). Figures 4.16. and 4.17. summarize susceptibility curves

for different magnetic fields with direction first along the lattice parameter a and then along c.

In terms of the magnetic field applied along a, curves were measured both for increasing and decreasing temperature. As the result, we can see that there is just one place with the difference between these two curves. This area is shown in the inset of Figure 4.17. In the reminder of the region of measurement, the curves are nearly the same. The only exception is the weak magnetic field 0.01 T, which lies lower than other curves.

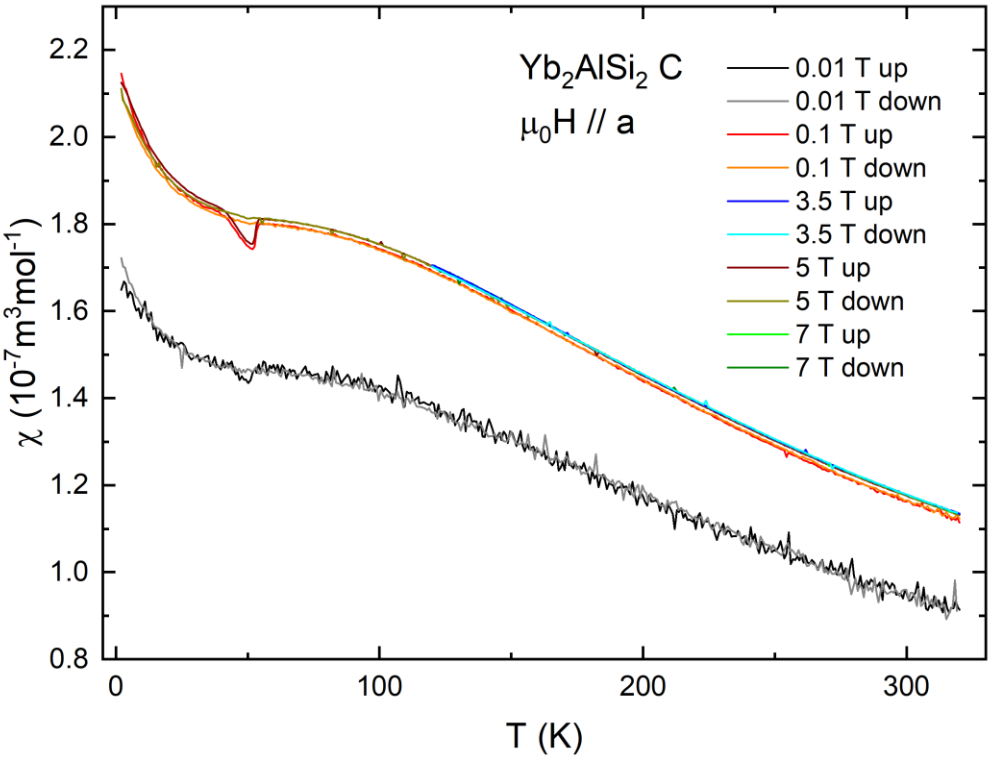

Figure 4.16. Temperature dependence of magnetic susceptibility for various values of external magnetic field (increasing and decreasing) applied along lattice parameter a

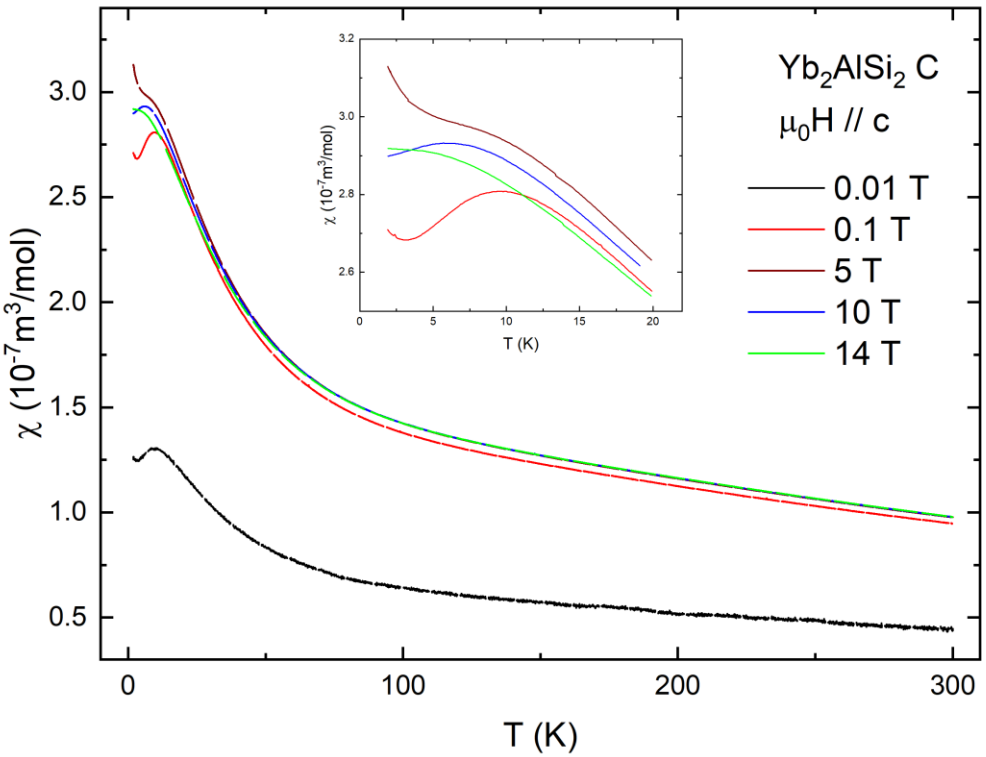

Figure 4.17. Temperature dependence of magnetic susceptibility for various values of external magnetic field applied along lattice parameter c

Also here, for the magnetic field along c, we can see that all curves apart from 0.01 T curve are nearly the same. As the consequence we got the same values of fitted parameters from Curie-Weiss law. This is described below. Interesting is the low temperature region below 10 K as is shown in the inset. The origin of this anomaly is not completely clear at the moment although it is reasonable to expect that the magnetic field is influencing the valence state of Yb which can be near the magnetic criticality.

In the paramagnetic state, behaviour of the sample is described by Curie-Weis law. (equation (1.9)). In studied crystal, we can observe paramagnetic behaviour for temperatures above 210 K for field along a and above 140 K for field applied along c. At this temperature regions, measured data obey Curie-Weiss law very well. Data from the temperature interval between 210 and 320 K for field along a (140 K and 300 K for field along c) were fitted with the function according equation (1.9) using software OriginPro. This is shown in Figures 4.18 and 4.19 including also the graph of inverse susceptibility, which can be fitted with the linear function in the paramagnetic region of the sample behaviour. Using formula (1.10) we can get values of effective magnetic moment μ_{eff} for the formula unit, which contains two

atoms of ytterbium. The μ_{eff} for one atom of ytterbium will be just a half. The following Tables 4.1. and 4.2. contain the results of fitting for each value of $\mu_0 H$ for both orientations of external magnetic field.

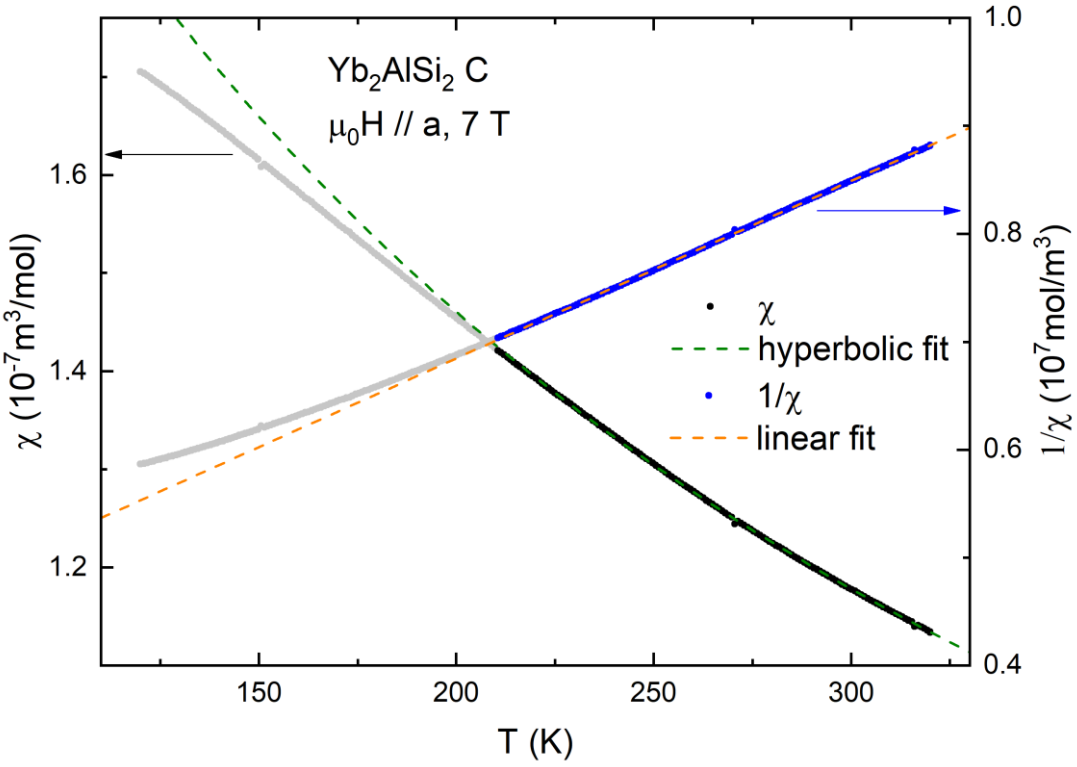

Figure 4.18. Magnetic susceptibility with hyperbolic fit by Curie-Weiss law and inverse magnetic susceptibility with linear fit for magnetic field 7 T applied along lattice parameter a and temperatures over 210 K

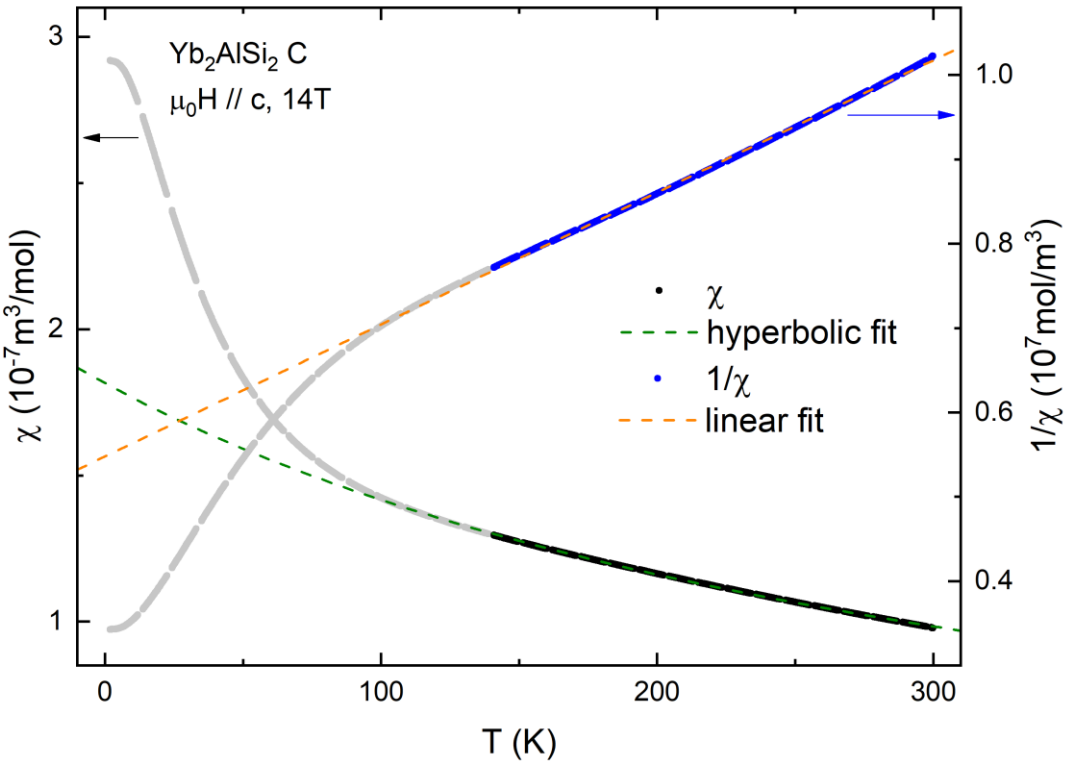

Figure 4.19. Magnetic susceptibility with hyperbolic fit by Curie-Weiss law and inverse magnetic susceptibility with linear fit for magnetic field 14 T applied along lattice parameter c and temperatures over 140 K

Table 4.1. Results of hyperbolic fits of susceptibility temperature dependence in the paramagnetic region 210 K – 320 K for external field applied along the lattice parameter a

	$\mu_0 H \,//\, a$			
$\mu_0 H$ (T)	μ_{eff} (μ_B/Yb)	$\sigma_{\mu_{eff}}$ (μ_B/Yb)	θ_P (K)	σ_{θ_P} (K)
0.01	2.83	0.36	-230.7	8.0
0.1	3.07	0.15	-211.0	1.1
3.5	3.12	0.10	-219.7	0.5
5	3.11	0.08	-217.1	0.3
7	3.11	0.10	-217.2	0.5

Table 4.2. Results of hyperbolic fits of susceptibility temperature dependence in the paramagnetic region 140 K – 300 K for external field applied along the lattice parameter c

	$\mu_0 H \,//\, c$			
$\mu_0 H$ (T)	μ_{eff} (μ_B/Yb)	$\sigma_{\mu_{eff}}$ (μ_B/Yb)	θ_P (K)	σ_{θ_P} (K)
0.01	2.18	0.12	-369.1	1.8
0.1	3.15	0.08	-355.0	0.3
5	3.19	0.08	-353.4	0.4
10	3.20	0.09	-354.6	0.4
14	3.20	0.11	-354.9	0.6

For both directions of magnetic field we can see that for the lowest magnetic field 0.01 T, using the Curie-Weiss law doesn't give reasonable results and for higher fields, we get similar effective moments for each measurement. These values of μ_{eff} correspond well to each other within the error of measurement. Compared with a theoretical $\mu_{eff} = 4.54\ \mu_B$ for ytterbium, the experimental value is smaller, which would reflect the valence fluctuation of Yb ion. The average effective moment for the higher fields (excluding 0.01 T) is $\mu_{eff}^{a} = (3.11 \pm 0.10)\ \mu_B$ for field along a and $\mu_{eff}^{c} = (3.19 \pm 0.09)\ \mu_B$ for field applied along c. When we assume that the smaller experimental value of μ_{eff} is caused by mixing of magnetic valence state 3+ and nonmagnetic 2+, we can estimate the ratio Yb^{3+} : Yb^{2+} to be $47:53$ for field along a and $49:51$ for field along c from the μ_{eff} ratio squared of $(3.11/4.54)^2$ respectively $(3.19/4.54)^2$ [26]. The obtained ratio give the estimate of Yb valence in the studied compound as 2.47+, when the field direction is along a and 2.49+, when the field points along c.

In terms of temperatures θ_P, if we exclude the lowest external field 0.01 T (according to results for effective moment), we get the mean values for higher fields as $\theta_P^a = (-216.3 \pm 3.7)$ K and $\theta_P^c = (-354.5 \pm 0.9)$ K. The large, negative θ_P is a characteristic feature of spin/valence fluctuation [2].

4.4. Heat capacity measurement

Measurement of heat capacity was carried out on monocrystalline sample Yb_2AlSi_2 C. First, the heat capacity temperature dependence in zero magnetic field was measured. Studied temperature range was 2 K – 320 K. In this range, only the zero field curve was measured. Curves for non-zero external magnetic field (for each value the field was applied along parameter a) were measured for temperatures from 2 K to 60 K for field 0.1 T and to 40 K for remaining fields.

In the following graphs, the curves of heat capacity temperature dependence are shown. Figure 4.20. shows the dependence in the whole temperature range. In the inset, we can see all curves for temperatures below 40 K. We can see, that for values of applied magnetic field curves merge. For the better clarity, also the dependence of C/T on T^2 for $T^2 < 1600$ K^2 and for $T^2 < 400$ K^2 were drawn (Figures 4.21. and 4.22.). Here we can observe the anomaly in small temperatures. Around 6 K, there is

a local maximum in C/T curve, which is usually associated with the presence of heavy-fermion ground state [29].

Over this anomaly, for temperatures $300 < T^2 < 600$, curves obey the Debye T^3 model for low temperatures very well. The data were fitted using mentioned model according to the relation (1.15). The fitted curve is shown in C/T function of T^2 graph in Figure 4.23. In these axes, the Debye model predicts the linear dependence.

Table 4.3. Results of linear fits of specific heat temperature dependence in the region of small temperatures 17.3 K – 24.5 K for various values of external field applied along the lattice parameter a

$\mu_0 H$ (T)	θ_D (K)	γ_0 (mJ mol^{-1} K^{-2})	σ_{γ_0} (mJ mol^{-1} K^{-2})
0.01	168.9	152.0	0.8
0.1	168.8	152.6	0.9
1	168.9	152.6	0.8
3.5	168.8	152.2	0.9
5	168.9	152.5	0.8
10	169.5	154.3	1.0

Values correspond well to each other within the error of measurement (error of θ_D is negligible). Only the values for 10 T field are little bit higher. As the mean value of data in previous Table 4.3., we get final $\theta_D = (168.8 \pm 0.1)$ K and $\gamma_0 = (152.7 \pm 1.2)$ mJ mol^{-1}K^{-2}. This enhanced value of Sommerfeld coefficient together with observation of a local maximum as mentioned above supports the evidence of heavy-fermion ground state.

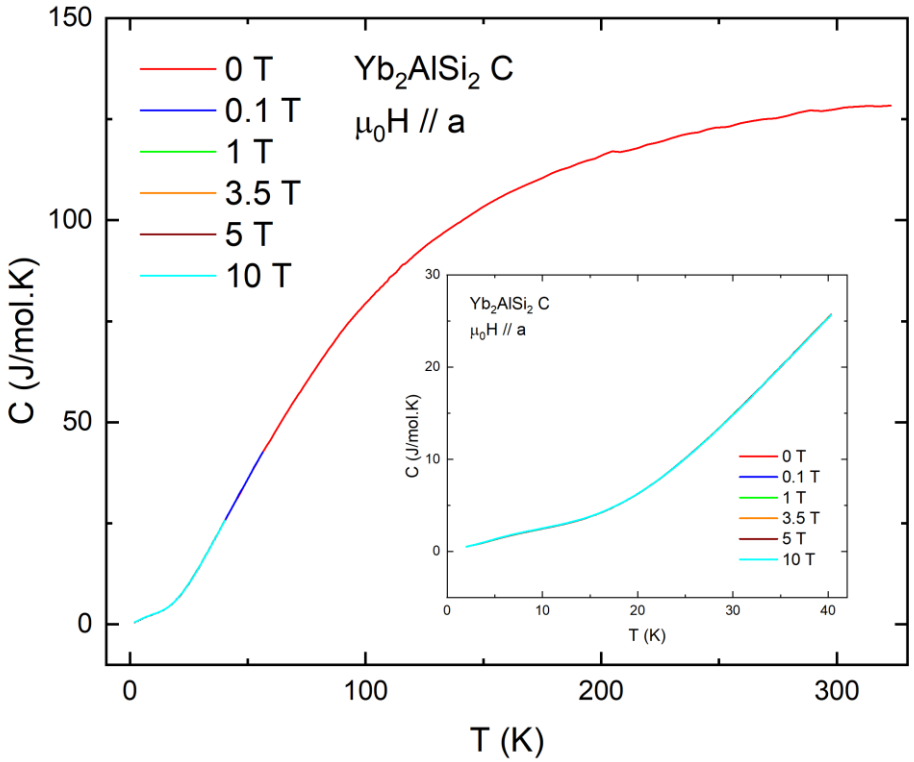

Figure 4.20. Heat capacity temperature dependence for various external magnetic fields applied along lattice parameter a with detail of the dependence for small temperatures in the inset

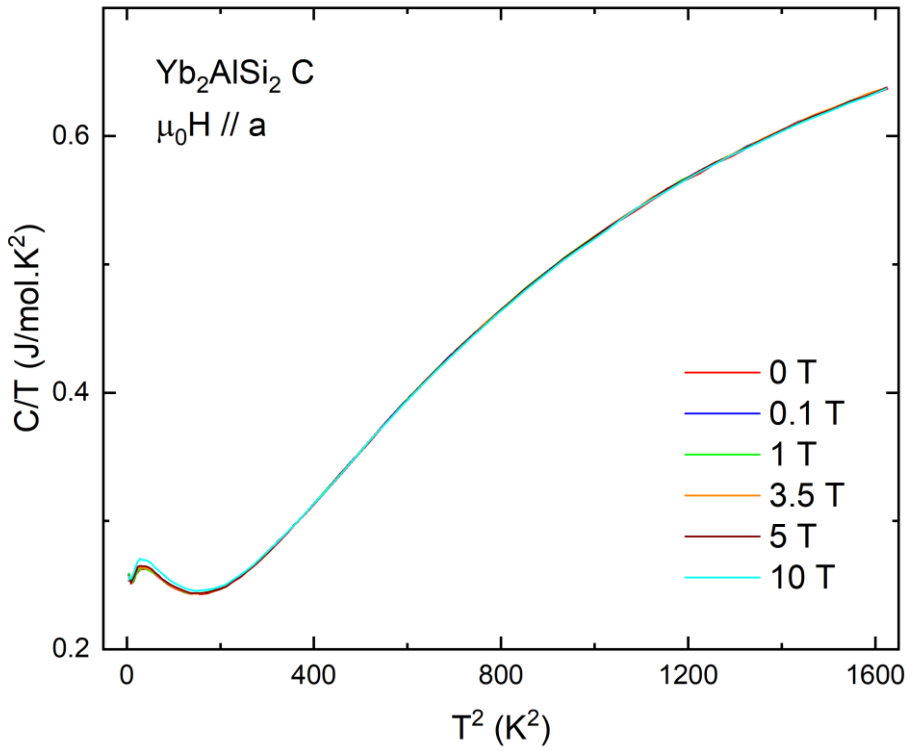

Figure 4.21. Heat capacity temperature dependence in axes C/T and T^2 for various external magnetic fields applied along lattice parameter a for temperatures under 40 K

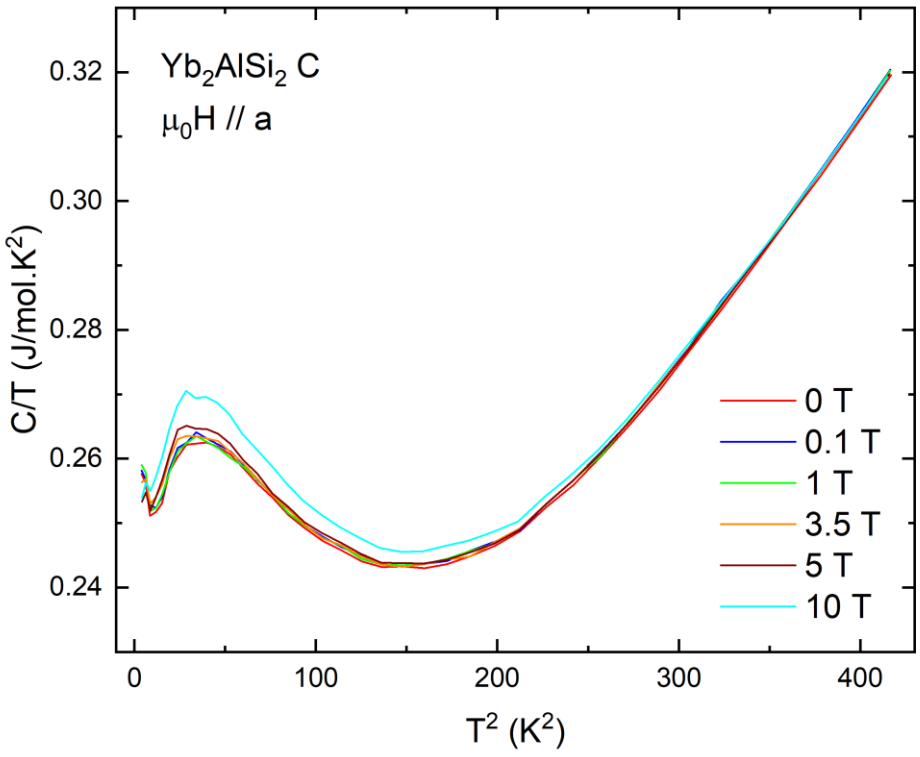

Figure 4.22. Heat capacity temperature dependence in axes C/T and T^2 for various external magnetic fields applied along lattice parameter a for temperatures under 20 K with well visible anomaly

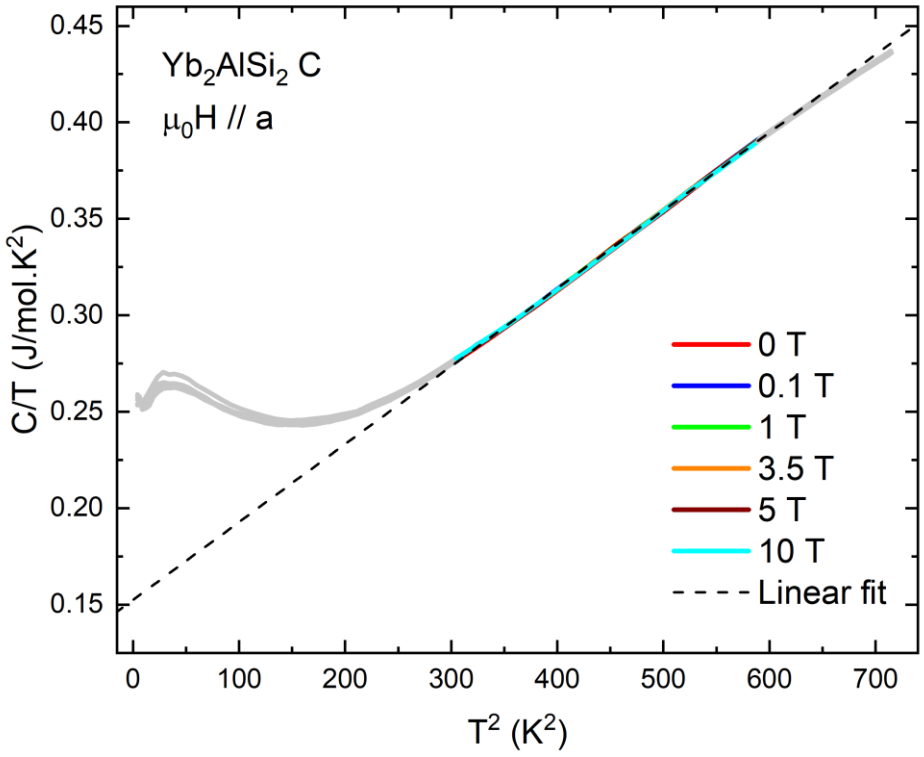

Figure 4.23. Heat capacity temperature dependence in axes C/T and T^2 for various external magnetic fields applied along lattice parameter a with linear fit according the Debye T^3 law (fit shown in graph is for 5 T curve)

4.5. Discussion

All measurements were carried out on monocrystalline samples. The main advantage with respect to previously studied polycrystalline samples is the fact that we can study the physical properties with respect to the crystal anisotropy. From X-ray diffraction the expected crystal structure and orientation were checked. The EDX analysis confirmed the homogeneity and purity of samples selected from the set of crystals prepared by method of growth from alumina flux. We obtained results that confirmed these properties well. In X-ray powder diffraction pattern, there appear two peaks that don't belong to the structure P4/mbm. This fact may coincide with also the EDX analysis. EDX analysis shows very good homogeneity and phase purity, but the stoichiometry obtained from the point analysis isn't exactly $2:1:2$. This fact can be the reality as the consequence of the thermodynamics during the crystal growth, but it can be also caused due to inaccuracy of analyzing method, because the fitted spectral peaks of detected elements are overlapping.

As for the measurements themselves, none of the measured curves did show any transition. The samples don't show the superconductivity transition in resistivity measurement, in magnetization measurements, there is no trace of magnetic ordering. All properties are evolving in temperature without the jump change. These results were confirmed by the heat capacity temperature dependence, where we also didn't observe any significant peak.

In comparison with previous results [2] obtained for polycrystal Yb_2AlSi_2, the resistivity temperature dependence for both current directions shows similar curve shape with the weakly changing resistivity in higher temperatures, but the values of resistivity, which was in our studies calculated only for current along c, are about six times smaller. This is probably caused by the monocrystalline nature and it also shows the higher quality of our crystal.

As for magnetization measurements, we confirm the paramagnetic behavior in temperatures over 200 K. The difference is that we could make experiment with external magnetic field applied both along a and c. The paramagnetic behavior was observed for temperatures above 210 K with field along a and in the second field direction above 140 K. The shape of susceptibility curve is again similar for polycrystalline and monocrystalline samples. The only difference appears in low

temperatures under 10 K for field along c and in temperatures around 50 K for field applied along a. The shape of the first mentioned anomaly is different for each magnetic field. There are also differences for zero-field cooled and field cooled measurements. We wanted to confirm that the shape depends on mentioned experimental detail, that's why all curves for field along a were measured both for zero field cooled and field cooled regime. But in this field direction, these anomalies didn't appear. Instead of it, there appeared the anomaly in higher temperature (around 50 K) which depends on the direction of temperature change (heating or cooling). This anomaly was observed for all values of external magnetic field. Suggested explanation may include the possibility of valence fluctuations present in the sample. This fact is corroborated by the estimated values of paramagnetic temperature, which were found to be large and negative ones.

Magnetic susceptibility data were fitted using a simple Curie-Weiss law (eq. 1.9). From fitting we obtained the values of effective magnetic moment with field along two directions $\mu_{eff}^{a} = 3.11\ \mu_B$ and $\mu_{eff}^{c} = 3.19\ \mu_B$ for one ytterbium atom. These values are smaller than $\mu_{eff}^{poly} = 4.2\ \mu_B$ obtained for polycrystalline sample. Also in the θ_P temperature are significant differences. In our studies we get values $\theta_P^{a} = -216$ K and $\theta_P^{c} = -355$ K. The previous result for polycrystal is $\theta_P^{poly} = -203\ K$. Obtained results are typical for spin/valence fluctuating Yb compounds in which the strong 4f conduction electron hybridization destabilizes the 4f-derived local moment and gives rise to a Pauli paramagnetic ground state.

As for the heat capacity measurement, we observed an anomaly with the local maximum in C/T below 15 K. An anomaly at low temperatures was observed also on polycrystalline sample by Shah et al. [2], but only as an upturn without the presence of the maximum. Except for the maximum at lowest measured temperatures observed in our case, the remaining curvature agrees well with that observed by the authors of the mentioned paper and was observed for some other heavy-fermion intermetallics. Nevertheless, similarly to Shah we are also not able to offer better explanation of this effect in present stage of study. It remains as a question for further studies of this interesting compound.

Conclusion

The thesis deals with the characterisation of the intermetallic compound Yb_2AlSi_2. Electric, magnetic and thermal properties were obtained for monocrystalline samples with respect to crystal anisotropy. The structural parameters were measured by powder diffraction. The summarized results follow.

Study of the crystal structure showed that the main control parameter for tetragonal P4/mbm lattice temperature evolution is a. On the other hand, the temperature changes in parameter c are nearly negligible.

Measurements of electric transport properties were performed in transversal arrangement (external magnetic field was applied along a perpendicularly to the current) and certain anisotropy for different directions of current were observed. The interesting behaviour appeared for current along a. No trace of any phase transition was observed.

In terms of magnetic properties, we can say, that studied compound exhibits paramagnetic behaviour, with tiny anomaly for external magnetic field applied along c, which disappears for higher temperatures. From the Curie-Weiss fits we obtained values of effective magnetic moments per one ytterbium ion $\mu_{eff}^{a} = 3.11\ \mu_B$ and $\mu_{eff}^{c} = 3.19\ \mu_B$ and large negative values θ_P temperatures $\theta_P^a = -216$ K and $\theta_P^c = -355$ K. No trace of magnetic ordering in the whole temperature and field region was observed. The anomaly of unknown origin observed in the specific heat below 15 K and peculiar evolution of magnetization whit respect to applied magnetic field needs further investigation in order to estimate its nature. In the temperature range from 17 K to 25 K, specific heat data follow the Debye T^3 model well. From fitting we got values of $\theta_D = 168.8$ K and $\gamma_0 = 153$ mJ mol^{-1}K^{-2}. These values suggest the heavy fermion ground state of Yb_2AlSi_2.

Bibliography

[1] KAŠTIL J., MÍŠEK M., KAMARÁD J., ARNOLD Z., VLÁŠKOVÁ K., PRCHAL J., DIVIŠ M., DOLEŽAL P., PROKLEŠKA J., VALENTA J., FIKÁČEK J., RUDAJEVOVÁ A., KRIEGNER D. *Properties of the divalent-Yb compound $YbAu_2Si_2$ under extreme conditions*. Physica B 505 (2017), 41-44

[2] SHAH K.V., BONVILLE P., MANFRINETTI P., WRUBL F., DHAR S.K. *The $Yb_2Al_{1-x}Mg_xSi_2$ series from a spin fluctuation (x = 0) to a magnetically ordered ground state (x = 1)*. Journal of Physics: Condensed Matter 21 (2009), 176001

[3] *Rare earth elements*, [online].
The Future of Strategic Natural Resources, 27.2.2018.
Available on:
http://web.mit.edu/12.000/www/m2016/finalwebsite/elements/ree.html

[4] *The Periodic Table of Elements*, [online]. 27.2.2018.
Available on: https://www.thinglink.com/scene/646518280235778049

[5] Wikipedia contributors. *Rare-earth element*, [online].
Wikipedia, The Free Encyclopedia, 27.2.2018, Last change 20.2.2018.
Available on: https://en.wikipedia.org/wiki/Rare-earth_element

[6] PRCHAL, Jiří, 2002, Prague. *Experimentální studium elektronových vlastností systému $RT_{1-x}T'_xAl$*. Master thesis. Charles University in Prague. Faculty of mathematics and physics.

[7] KITTEL, Charles. *Úvod do fyziky pevných látek*. 1. vydání, Academia, Praha, 1985

[8] Wikipedia contributors. *Ytterbium*, [online].
Wikipedia, The Free Encyclopedia, 27.2.2018, Last change 21.1.2018.
Available on: https://en.wikipedia.org/wiki/Ytterbium

[9] VLÁŠKOVÁ, Kristina, 2016, Prague. *Magnetic excitations in cerium compounds*. Master thesis. Charles University in Prague. Faculty of mathematics and physics.

[10] NAVE, R. *Resistivity and Conductivity*, [online].
HyperPhysics Concepts, Georgia State University. 8.3.2018.
Available on: http://hyperphysics.phy-astr.gsu.edu/hbase/electric/resis.html

[11] Wikipedia contributors. *Magnetism*, [online].
Wikipedia, The Free Encyclopedia, 11.3.2018, Last change 6.3.2018.
Available on: https://en.wikipedia.org/wiki/Magnetism

[12] Wikipedia contributors. *Diamagnetism*, [online].
Wikipedia, The Free Encyclopedia, 11.3.2018, Last change 18.2.2018.
Available on: https://en.wikipedia.org/wiki/Diamagnetism

[13] LATOŇOVÁ, Věra, 2015, Praha. *Charakterizace monokrystalu RCO_2*. Bakalářská práce. Univerzita Karlova v Praze. Matematicko-fyzikální fakulta.

[14] *Magnetism*, [online]. 25.3.2018.
Available on: http:// grund-wissen.de/physik/_images/diamagnetismus-paramagnetismusferromagnetismus.png

[15] *Definitions of ferromagnetic: Synonyms, Antonyms and Pronunciation*, [online]. DigiPaul, 2018, 25.3.2018. Available on: http://muchongimg.xmcimg.com/data/edu/a0/e9/177844_1307454878_460.gif

[16] *Heat capacity*, [online].
Chemistry LibreTexts, 13.3.2018, Last change 9.2.2017.
Available on: https://chem.libretexts.org/Core/Physical_and_Theoretical_Chemistry/Thermodynamics/Calorimetry/Heat_Capacity

[17] Wikipedia contributors. *Heat capacity*, [online].
Wikipedia, The Free Encyclopedia, 13.3.2018, Last change 20.2.2018.
Available on: https://en.wikipedia.org/wiki/Heat_capacity

[18] PIKUL A., TROĆ R., CZOPNIK A., NOËL H. *Low-temperature specific heat of uranium germanides.* Journal of Magnetism and Magnetic Materials 360 (2014), 217-221

[19] VALVODA Václav, POLCAROVÁ Milena, LUKÁČ Pavel. *Základy strukturní analýzy*. 1. vydání, Univerzita Karlova, Praha, 1992

[20] KRIEGNER D., MATĚJ Z., KUŽEL R., HOLÝ V. *Powder diffraction in Bragg-Brentano geometry with straight linear detectors*. Journal of Applied Crystallography 48 (2015), 613-618

[21] Optická versus elektronová mikroskopie, [online].
ZFP MFF UK, Praktikum III pro OF. Úloha 31, studijní text. Available on: https://physics.mff.cuni.cz/vyuka/zfp/_media/zadani/texty/txt_331.pdf

[22] QUANTUM DESIGN. *Physical property measurement system*, *Electrical Transport Option (ETO) User's Manual*. Fourth edition, 2013, San Diego, USA

[23] QUANTUM DESIGN. *Physical property measurement system*, *Vibrating sample Magnetometer (VSM) Option User's Manual*. Fourth edition, 2008, San Diego, USA

[24] QUANTUM DESIGN. *Magnetic Property Measurement Systém. User's Manual*. Third edition, 2004, San Diego, USA

[25] SKOROKHOD Yuriy, 2008, Prague. *Pressure effects on the magnetocaloric $R_5(Si_xGe_{1-x})_4$ compounds*. Doctoral thesis. Institute of Physics. Academy of Sciences of the Czech Republic.

[26] MITSUDA A., YAMADA K., SUGISHIMA M., WADA H. *Pressure effect on valence fluctuation and magnetic ordering in YbPd*. Physica B 404 (2009), 3002-3004

[27] FERNANDEZ-PANELLA A., BRAITHWAITE D., SALCE B., LAPERTOT G., FLOUQUET J. *Ferromagnetism in $YbCu_2Si_2$ at high pressure.* Physical Review B 84 (2011), 134416

[28] CARVAJAL J. R. *Recent advances in magnetic structure determination by neutron powder diffraction.* Physica B 192 (1993), 55-69

[29] REBELSKY L., REILLY K., HORN S., BORGES H., THOMPSON J. D., WILLIS J. O., AIKIN R., CASPARI R., BREDL C. D. *Heavy fermion behavior in CePtSi and CeRuSi*. Journal of Applied Physics 63 (1988), 3405

List of Tables

List of Abbreviations

REE	Rare earth element
XRD	X-ray diffraction
BSE	Backscattered electrons
SE	Secondary electrons
EDX	Energy dispersive analysis
PPMS	Physical Property Measurement System
ETO	Electrical Transport Option
VSM	Vibrating Sample Magnetometer
MPMS	Magnetic Property Measurement System
SQUID	Superconducting Quantum Interference Device
QCP	Quantum critical point